Department of Precision and Microsystems Engineering

Production, design and control of P(VDF-TrFE-CTFE) relaxor-ferroelectric actuators

R.J.P. van der Nolle

Report no   : 2017.023
Coach   : Dr. S.H. Hossein Nia Kani
Professor   : Prof. dr. ir. Just L. Herder
Specialisation : MSD
Type of report : Thesis
Date   : 07-03-2017

TU**Delft** Delft
University of
Technology

Challenge the future

Abstract

The amount of research and development in smart materials is increasing every year. These smart materials offer a solution to integrated and distributed actuation and sensing. Pressure sensors, acoustic transducers, deformable mirrors, micro-robotics and stiffness control of flapping wings are some applications where these smart materials show great promise over their external actuated counterparts. New materials are developed and reported regularly, P(VDF-TrFE-CTFE) a relaxor-ferroelectric polymer is such a smart material. Relaxor ferroelectric materials can convert electrical signals to mechanical strain and vice versa, allowing the possibility to act as an actuator and sensor in one. This relatively new material has some promising parameters, with a dielectric constant of 50, Young's modulus of 0.4 GPa, coupling factor of 0.3 and transparency above 88%, where 100% is no disruption of light at all. With these properties P(VDF-TrFE-CTFE) can serve as a useful component in mechatronic systems. In this thesis, the possibilities in production and enhancement of P(VDF-TrFE-CTFE) are discussed and experimentally validated. The piezoelectric and electrostrictive response in such polymers are formed through polarisation and annealing processes. This thesis shall prove as a guide to achieve the maximum electromechanical performance of a relaxor-ferroelectric polymer, a new method to successfully polarise this relaxor ferroelectric polymer is presented and a novel way to remove residual stresses after spin casting of thin film polymers is proposed.

Acknowledgement

Contents

List of Symbols

Symbol	Quantity	Unit
C	Flexural rigidity	Nm^2
d_{jq}	Piezoelectric coefficient	mV^{-1}
D_i	Components of electric Displacement	Cm^{-2}
d_{ikl}	Air gap	m
E_i	Components of electric field	Vm^{-1}
h	Thickness of layer	m
$h_{o,i}$	Upper distance of the ith layer from the neutral axis	m
$h_{u,i}$	Lower distance of the ith layer from the neutral axis	m
I	Moment of inertia	m^4
l	Length of the bending actuator	m
k_m	Wavenumber of the mth eigenmode	m^{-1}
M	Bending moment	Nm
m_{piezo}	Piezoelectric moment per voltage	NmV^{-1}
n_0	Translatory reference compliance	mN^{-1}
n_m	Torsional compliance	N^-1m^{-1}
P_{xy}	Cross spectral density x y	$-$
P_{xx}	Power spectral density x	$-$
Q_m	Q-factor	1
r	Radius	m
r	Coefficient of friction	Nsm^{-1}
S_{pq}^E	Elastic compliances at constant electric field	m^2N^{-1}
S_{ij}	Strain tensor	$-$
t	Time	s
T_{ij}	Stress tensor	Nm^{-2}
U	Internal Energy	Jm^{-3}
u	Voltage	V
u_{piezo}	Input voltage per electrode	V
w_i	Width of the ith layer	m
w_{tot}	Total energy density	Jm^{-3}
x	Distance	m
X_m	Eigenmode, Eigenfunction	1
Y	Gyrator constant	C^{-1}
$\bar{z}$	Neutral axis position	m
ω	Frequency	s^{-1}
ω_m	Eigenfrequency	s^{-1}
ε_{ik}	Permittivity tensor	Fm^{-1}
μ	Mass per unit length	kgm^{-1}
ξ	Deflection	m
θ	Temperature	K,°C
Σ	Entropy	JK^{-1}

1

Introduction

Smart materials offer a way to replace external actuators [1] or sensors [2] from systems. By integrating a smart material onto the surface of a system, motion can be generated [3]. These smart materials can be compared to live muscles [4]. Muscles convert chemical energy intro mechanical energy by exhibiting strain, smart materials can do something similar when activated with an external stimulus, electric voltage or heat for example. The last decades many new smart materials are researched and some show great promise for future applications where an external actuator is not preferred [5].

Smart materials can be found in many physical domains, the general idea is the transfer of energy from one domain to another. Examples of these different or combined domains can be found in light [6][7], chemical [8], heat [9], magnetic [10], pressure [11][12] and electric [1]. While each of these domains can have their advantages, they most certainly also have their disadvantages, think of high voltages, large magnetic fields or specific operating frequencies. In the selection of a smart material the application plays a key factor.

P(VDF-TrFE-CTFE) is a good example of such a material which has a mechanical output as a result of an electrical input. The material where P(VDF-TrFE-CTFE) is based on is P(VDF-TrFE). Actuators made from P(VDF-TrFE) exist in many forms and applications, a decade ago it has received an upgrade to P(VDF-TrFE-CTFE)[13]. With this upgrade, the electromechanical response has increased from 0.1% strain to a maximum of 3.5% strain[14]. Time to see what the possibilities are regarding applications with this new material. The change in this new type of polymer is found in the molecular structure of the material. By adding Chloride atoms to the polymer chain, defects are introduced. these defects increase the electromechanical behaviour[15], lower curie-temperature, reduce hysteresis and provide spontaneous polarisation. Although some features are significantly enhanced, the Youngs modulus is lowered from 3.3GPa to 0.4GPa, making the material suitable for high deflections but reducing its possibility for high blocking forces.

In this thesis, the production steps and verification of a cantilever type of actuator using the electro to mechanical domain with a ferroelectric polymer will be discussed. This polymer is flexible for different designs since it can be cast into any thickness and cut into any shape[16][17][18][19]. Modifications during the production process can influence the electromechanical performance. Some of these modifications are tested and documented in this thesis, supplying a good basis for engineers looking to build their own applications with a ferroelectric polymer material. While the material has a bright future ahead production is not that straightforward. In this thesis, all steps required to successfully create a ferroelectric single layer polymer actuator will be discussed and an example shall be presented.

At the TUDelft more research in smart materials is appearing [20], compliant mechanisms and origami are a known principle [21][22][23]. The actuation of these compliant mechanisms is often done with large external actuators, by using thin film polymer actuators inside these compliant systems those external actuators are deemed futile. While origami shows great potential in many applications [10][24], self-folding is a research area not widely explored in 3ME - PME. The ability to cast a thin layer of polymer on an origami structure to turn it from dumb to smart, enabling the ability to fold itself will change the role of origami completely within the faculty.

Residual stress in thin film polymers can cause problems in small and large scale applications[25][26]. A strain of 0.5 percent and up can make MEMS device application bend into undesired shapes[27]. Surfaces coated with polymers for protection or active layers with internal stress can cause cracks, like paint on a surface that cracks over time[28]. These cracks are formed when the whole solvent is evaporated and the

sample is completely dried. Multiple researchers [26][29] state that the cause of residual stress as a result of spin casting is induced by the high evaporation rate where the wet polymer is exposed to. The polymer chains are forced to bond together as the solvent evaporates, creating undesired polymer chains. It has been shown in this thesis that a process step to completely remove the residual stress induced by spin casting is possible. This is an important step indeed and it is easy to perform with tools and equipment readily available.

Finally, a new method will be presented for the polarisation of ferroelectric polymers to increase the piezo-electric effect and electrostrictive response without heating up the polymer. The polarisation of polymers increases their electromechanical response. Most often this polarization is done by heating up the material, enabling the internal polymer chain to reorient its position, and applying a DC voltage to get a preferred position. This new method allows the possibility to polarise ferroelectric polymers integrated in a system where other parts of this system would be vulnerable to temperature changes.

2

Ferroelectric Polymers

In 1963 the first ferroelectric polymer was synthesised by Kocharyan[30]. Kocharyan published two organic polymers, poly(methyl methacrylate) and poly(vinyl chloride). These materials piezoelectric properties were enhanced by Kawai in 1969[31] by introducing stretching and temperature increased methods. It was in 1971 that the ferroelectric properties of PVDF were shown by Nakamura [32], opened a path to a field of research in ferroelectric polymers. It was known for a while that by introducing defects the ferro-electric properties of these polymers can be increased drastically. These defects are introduced with electron radiation [33][34]. The last decade a new polymer recipe has shown great potential in increasing ferroelectric and piezoelectric effects, combining the idea of defects in the material and avoiding electron radiation to have a positive effect on both the electrical and electromechanical response [35].

2.1. Piezoelectric effect

Piezoelectric effect - translated from Greek, (piezein = press + electric effect), the effect to produce electricity with pressure. Crystal structures which do not have a symmetric crystal lattice, concerning the positive and negative ions of the molecule, have this piezoelectric effect. By deformation of the crystal the positive and negative ions create an electric charge perpendicular or parallel to the pressure direction [36], this is graphically displayed in figure 2.1. This effect is also reversible, called the inverse piezoelectric effect. With the inverse piezoelectric effect, an electric charge or potential difference will force the crystal structure to deform, creating strain in the material volume.
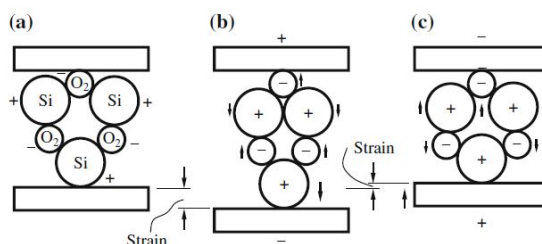

Figure 2.1: Piezoelectric effect explained with silicon and oxygen atoms. In rest(a) there is an equilibrium between the positive and negative ions. under tension(b) or pressure(c), the equilibrium is disturbed and a current is allowed to flow.

2.1.1. Ferroelectric effect

Ferroelectricity is a form of piezo-electricity, in which the electrical energy is converted/stored to/in mechanical or chemical energy by internal deformation of the material at the molecular level. Positive and negatively charged atoms can rotate around the polymer backbone under the influence of an electric field.

The polarity of piezoelectricity agrees with the assumption that the polarisation is due to dipole orientation in the crystal. Furthermore, it was shown by experiment that the polarity of piezoelectricity is reversed by the reversed poling. Therefore such a material can be called ferroelectric [32].

Reversibility of the polarisation is the key factor which identifies ferroelectric materials. The material molecule structure must have the ability to rotate around its axis by 180° if this cannot be achieved in a continuous fashion the material is not ferro-electric [37].

2.2. Polarization

Electrets are polarised materials that show positive and negative preference similar to magnetic material, [38]. This polarisation is generally done by heating up the solid material (making the material soft) and applying an electric field over the heated material. This way the atoms attached to the polymer backbone (for ferroelectric polymers) can rotate around to the preferred position. When the temperature is released the materials viscosity increases making it harder for the atoms to return to their original state, thus they will stay in the alignment of the electric field. This is how polymers become polarised. The amount of polarisation depends on many factors; the thickness of the material, the strength of the electric field, the temperature of the material during polarisation, time of polarisation, electrode material, steps taken to produce the material, etc. Some polarisation methods are described in Table 2.1. The polarisation will degrade over time and vanish if waited long enough, this could take seconds or years depending on earlier mentioned factors[37][39].

relaxor-Ferroelectric material can be characterised with so-called spontaneous polarisation, this material will show electromechanical response immediately after any form of the production process. The magnitude of polarisation is unrelated to production steps or polarisation, this is experimentally confirmed in this thesis.

The thermal polarisation time can be plotted with the empirical equation 2.1 depicted by Buchman [40], where J_{max} is the maximum current density, J_0 is the starting current, E is the electric field density, k is the Boltzmann constant T is the temperature and n and α are constants where n is varying from 0.7 to 1.6 and α is equal to 0.65eV.

$$J_{max} = J_0 E^n e^{-\alpha/kT} \tag{2.1}$$

2.3. Analogue to Magnets

Eguchi [47] was the first to make the analogue between magnets and electrets. Where magnets have a magnetic field, a north and south pole. Electrets have an electric field, a positive and a negative side. If an electret would be cut into two, two new electrets with the same properties would appear. Eldridge [48] showed that interactions between magnets and electrets are the same. However, these similarities exist there are also plenty of differences. Electrets are not found in nature, are destroyed upon heating up and the electret effect slowly fades in time. These decays are typical for electrets and are not observed in magnets [41]. Therefore, while the comparison with magnets is often made, they are not completely analogue.

2.4. Poly(VinyliDene Fluoride) - PVDF

PVDF, a common polymer which is well known for its durable material properties high mechanical and impact strength, resistance to abrasion, deformation and chemical de-evaluation. PVDF is machinable, cast-able and eligible for any other forms of production used for thermoplastics. Next to these mechanical properties it also is ferroelectric, enabling the possibilities of dielectric applications and smart actuation. combine the mechanical properties with ferroelectric properties and we have a special polymer with high potential[14].

PVDF, consists of two carbon atoms bound to either hydrogen or fluoride, ($-CH_2$-CF_2-). Defects in this material occur when this order is disturbed and ($-CH_2$-CH_2-) or ($-CF_2$-CF_2-) are formed, so-called head to head (HH) or tail to tail (TT) defects. Generally, these defects occur 4%-5% in commercial material and with good conditions can be synthesised with ranges from 0.2% to 23.5% [41]. These defects combined with the crystal structure of PVDF create electric dipoles in the material, creating the ferroelectric properties of PVDF. PVDF can have a crystal structure in four polymorphs, named α, β, γ and δ. α has the ($TGT\bar{G}$) conformation. β has the (TT) conformation. γ has the ($T_3GT_3\bar{G}$). in the δ-phase, the conformation is the same as in the α-phase, the difference is hidden in the dipole orientation, where the dipole moment in the δ is parallel orientated with respect to the molecules in the materials unit cell, while in the α-phase they are anti-parallel [41][49], the shape of these phases are graphically displayed in figure 2.2.

The effects of these different phases are found in the electrical and mechanical domain, since this thesis focus is in the mechanical actuation part the effects shall be discussed accordingly. When the material is in

Table 2.1: Polarization methods by Nalwa [41].

| Polarization method	Description
Thermal polarisation	As described above, this method makes use of the soft material properies combined with an electric field to polarise the material.
Ceramic polarisation	Ceramic materials can be polarised at much higher temperature, thus they have there specific method.
Photo polarisation	Specific designed for photo conductive materials, here an electric field is applied while the material is radiated with photons. This process is often accompanied by thermal steps.
Thermophoto polarisation	The combination of photo- and thermal polarisation.
Magneto polarisation	Some materials polarise better when there is an magnetic field joining the electric field, allowing the molecules to orient more neatly.
Corona charging	A method to polarise samples using an electric field induced by corona wires and a earth plate above and below the sample respectively. 8kV to 13kV voltage difference ensures a dense electric field on the sample [42]. This method only takes one second and can be executed at room temperature.
Charge injection	A quick and strong method to form electrets by using brush shaped electrodes close to a pre-heated sample. The combination of temperature and corona charges ensure strong polarisation [43].
Radio polarisation	A treatment for material that specifically responds to radiation [44].
Electron beam charging	is an excellent method to polarise non metallized polymers. Using an electron beam with the focus on the polymer layer large amounts of electrets can be formed very quickly[45]. this method is used extensively in industry these days [41].
liquid contact polarisation	When one side of the polymer film is metallized the other side can be put in contact wth a conducting liquid. When a potential is set on either the metalized surface or the liquid the polymer shall be polarised [46].
Mechanical compression	Pressurizing the material can also create electrets, they are forced into the material mechanically [41].
Solvent polarisation	This is a new method described in this thesis. Using the solvent to weaken the polymer structure, polarising the material without the need of increasing the temperature.
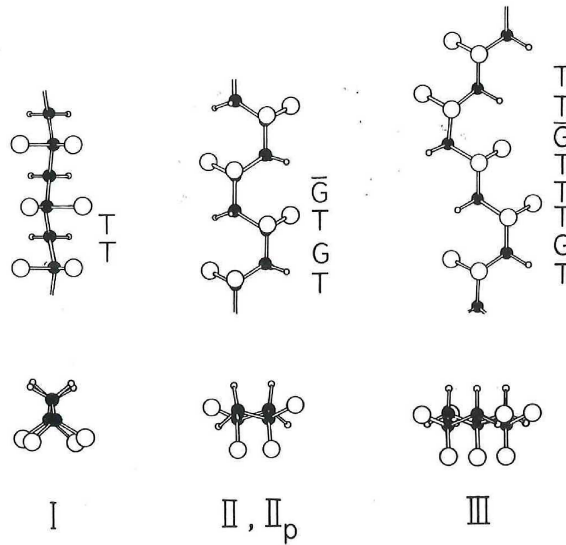
Figure 2.2: Molecular structure of the four pvdf phases, $\alpha = II$, $\beta = I$, $\gamma = III$ and $\delta = II_p$, this figure is directly adopted from H. Nalwa [41].
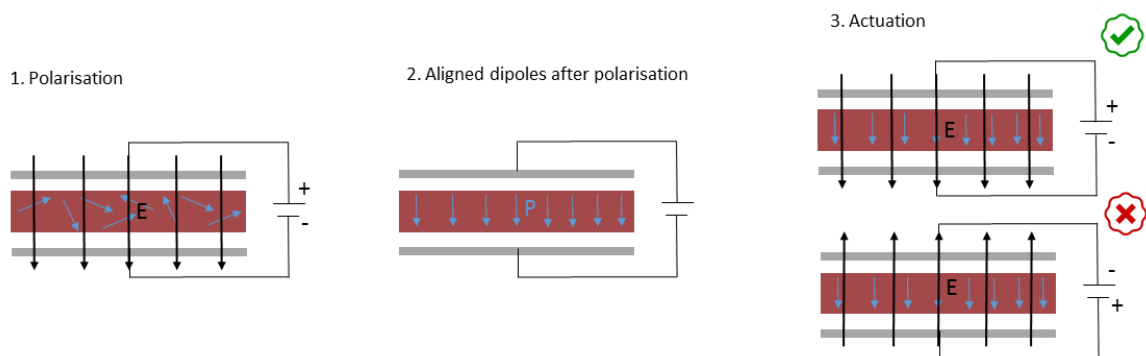

Figure 2.3: After polarisation (step 1) the dispoles in the material are aligned in a prefered direction (step 2), actuation should take place in the same direction to achieve maximum electromechanical response (step 3).

the alpha-phase it shall act as a paraelectric material, with as result that there is only a electrostrictive, uni-directional, response to an electrical input. This effect is also displayed in the polarisation of the material, figure 2.4a. After a polarisation step with electrical field E the polarisation state shall return to zero.

When the material is in the beta-phase it shall act as a ferroelectric material, with as result that there is also a piezoelectric, bidirectional, response to an electrical input. When the material is in the beta-phase the ferroelectric polarisation is possible, making it able to polarise the electric dipoles. When these dipoles are polarized the material has a preference actuation direction. An electrical input with the same sign (positive or negative) as the polarisation sign will result in a stronger deflection then when the actuation sign is opposite, see figure 2.3. This effect is measured and displayed in section 6.1.1 figure 6.5. The ferroelectric effect can also be displayed in the polarisation of the material, figure 2.4b. After a polarisation step with electric field E is removed, there is some remaining spontaneous polarisation P.

The polarisation of ferroelectric properties were first (1978) identified by Kepler and Anderson [50]. Using X-ray diffraction before and after polarisation steps, they confirmed the change in dipole orientation. This was later confirmed by Tamura et al. [51] and Naegele and Yoon [52] with infrared absorption studies.

A popular way to increase the β-phase is by stretching or rolling the material [53]. When the material is stretched the polymer chains in the α-phase are elongated and form a more β-phase shape. Since the β-phase is dominant in the electromechanical behaviour this method is favourable for applications. The

(a) paraelectric effect.
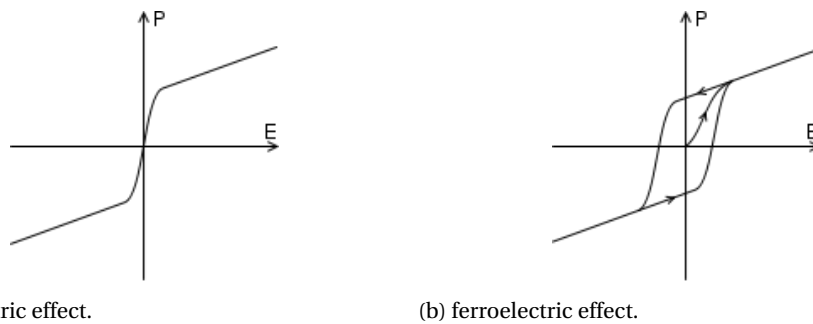
(b) ferroelectric effect.

Figure 2.4: Difference between paraelectric and ferroelectric effect. The ferroelectric effect has as resultant polarisation P when the electric field E is removed.

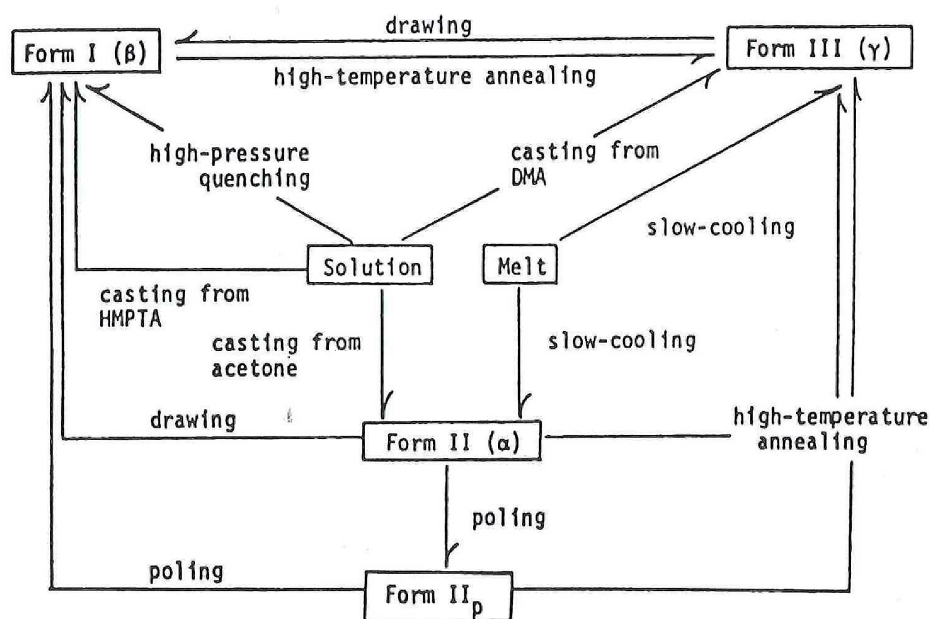methods possible to reach this and other phases are graphically displayed in figure 2.5.

Figure 2.5: Modifications to reach the desired crystalline structure, this figure is directly adopted from H. Nalwa [41].

2.4.1. Poly(VinyliDene Fluoride-TriFluoroEthylene) - P(VDF-TrFE)

The most common used ferroelectric polymer is P(VDF-TrFE). Introducing TrFE monomer into the polymer results in a larger unit cell, the volume increase results in a weaker intermolecular interaction between the VDF monomers. The effect of this separation, a larger distance between VDF monomers, can be found in the interacting dipole moments between the monomers. The interacting dipole moments are reduced [41]. The maximum achievable strain as a result of electrical input can be increased, from 0.1% [33], up to 5% [41] with different fabrication methods.

While the material has a strain of up to 0.1% [33], this can be improved by different fabrication methods.

Electron irradiation greatly improves the electromechanical and dielectric performance of P(VDF-TrFE), see fig 2.6. By bombarding the material with electrons, defects are constructed. These defects break up the default polymer all-trans chain into an alternating all-trans/gauche chain, this makes the polymer a relaxor ferroelectric [33]. The process of electron irradiation is unfortunately not as simple to perform. Advances have been made to add a third monomer to the structure to mimic the effects of electron irradiation, resulting in P(VDF-TrFE-CTFE) [14][54].
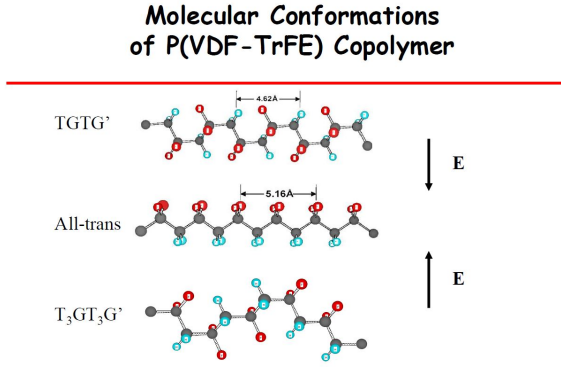
Figure 2.6: Conformation changes of P(VDF-TrFE) to order the molecular structure by electron radiation[54].
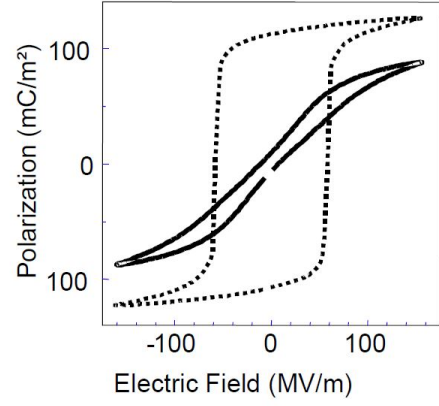

Figure 2.7: Hysteresis curve of normal ferroelectric polymer (dotted line) vs relaxor ferroelectric polymer (solid line)[54].

Figure 2.8: Improvements on P(VDF-TrFE)

2.4.2. Poly(VinyliDene Fluoride-TriFluoroEthylene - ChloroTriFluoroEthylene) - P(VDF-TrFE-CTFE)

By adding relative large chlorine atoms in the polymer imposes a large steric hindrance, relieve the repulsion forces between hydrogen and fluorine atoms. This has an effect that the dipoles off all monomer pairs added results in a higher polarisation [55]. The electrical energy stored in a polymer is related to this polarisation. Higher polarisation means better electromechanical performance. Next, to the polarisation increase and similar to the introduction of the TrFE monomer has the CTFE monomer to relieve the intermediate forces between the VDF monomers [15]. Leading to a relaxor ferroelectric which eliminates the polarisation hysteresis and dielectric heating, see figure 2.7. Summing these modifications we get a material with an electromechanical strain of 0.5% at 7v/μm and greater than 3.5% at 100 V/μm. This would correspond to a deflection in a cantilever of 2 by 15 mm, as will be presented in chapter 3, of 11μm to 150 μm at the tip. The presence of the CTFE atom lowers the Young's modulus from 3.3Gpa to 0.4Gpa which might limits the materials use [14][54].

The electromechanical coupling factor k_{31} is composed of the electrostrictive component and the piezoelectric component. Combining the electrostrictive strain, the elastic modulus and the polarisation data the electromechanical coupling factor squared measures the energy conversion efficiency from the electric to the mechanical domain. The electrostrictive component is derived as equation 2.2 where s_{11}^D is the elastic compliance, S_3 the measured strain in z-direction, P is calculated in equation 2.3,E the Young's modulus, P_s is the saturation polarisation which together with k_{31} can be depicted by a fit curve, k_{31} for P(VDF-TrFE-CTFE) is $0.25 - 0.3$ [35][56][57].

$$k_{31}^2 = \frac{kS_3^2}{s_{11}^D \left[Pln(\frac{P_s+P}{P_s-P})P_s ln\left(1-(\frac{P}{P_s})^2\right)\right]} \tag{2.2}$$

$$|P| = |P_s|\tanh(kE) \tag{2.3}$$

It has been previously shown that in the case of dielectric polymers, the electrostrictive strain under an electric field can be mainly attributed to Maxwell forces induced by dipolar orientation within the material [58]. In the thickness direction, the transverse strain S_{31} under the electric field E is given by equation 2.4 where E is the electric field and M_{31} is given by equation 2.5 where ε_0 is the relative permittivity of vacuum, ε_r is the relative permittivity of the polymer and Y is the Young's modulus of the polymer or equation 4.16 for multilayer systems [59].

$$S_{31} = M_{31} E^2 \tag{2.4}$$

$$M_{ij} = \frac{\varepsilon_0 \varepsilon_r}{Y} \tag{2.5}$$

3

Design

In this chapter every design considerations to build a cantilever type actuator is discussed. Every aspect of the cantilever is designed regarding maximum deflection for mini-size applications. Next to the performance of the actuator the equipment available at the TUDelft was taken into consideration.

3.1. Basic Capacitor Design

A capacitor is made of multiple unique or repeating layers. The top and bottom layers consist of conducting materials, making the electrodes. The centre layer is made of a dielectric material which stores the electric charge and transforms it to heat and strain. With this design, a uniform electric field can be generated in the dielectric material by setting a voltage potential on the electrodes. The flat electrodes ensure that the electric field density is constant over the dielectric layer.

The dielectric material shall deform under the influence of an electric field. This deformation is induced by the electrostrictive and piezoelectric material properties. To verify this strain we can convert it into bending motion. A capacitor alone shall not bend, it shall only contract or expand, another layer is required, a layer which has a strain in the opposite direction or which has a higher stiffness than the initial capacitor. The combination from either of these layers will turn the strain in the active layer into bending motion of the system.

3.2. Cantilever Design

The shape of the actuator is a thin cantilever of $15mm$ long and $2mm$ wide. These dimensions are chosen with the paper of E. Edqvist [60] in mind to create a similar cantilever for comparison purposes. The cantilever shall be clamped on the position where the electrodes shall be connected to a voltage source. The final design shall therefore be 'T' shaped, in this shape the cantilever is free to move and there is enough space to connect electrodes, see figure 3.1.

The final cantilever is made of four layers, these layers are explained next. First there is a substrate base layer, then there is an electrode layer, the active polymer layer and finally another Electrode, see figure 3.1.
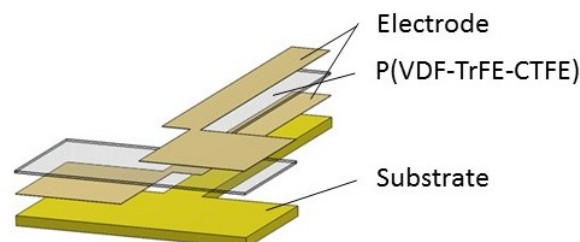

Figure 3.1: Simplified view of a cantilever design. The layer mentioned are Gold electrodes, 20nm thick. P(VDF-TrFE-CTFE) active polymer layer, $8\mu m$ thick and a polyimide substrate, $50\mu m$ thick.
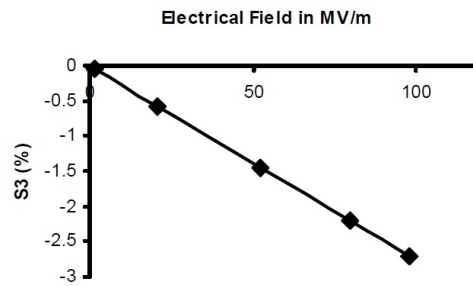
Electrical Field in MV/m

Figure 3.2: Longitudinal strain in stretched P(VDF-TrFE-CTFE)[62].

The electrodes have to be connected to a control circuit to be able to actuate the cantilever, this is achieved by making the T-shape electrodes. The electrodes are split left or right in the T-shape and can be connected to a wire with any clamping mechanism.

The thickness of the layers can be chosen by the designer, for a good conductance the electrodes should be thick enough for the selected material, the thickness also has an influence to the robustness of the actuator. For the actuators in this thesis, gold was chosen as electrode with a thickness of 20-40nm since this value has proven to be sufficient [18][61].

The thickness of the active polymer has influence on the output strain and output force, a thicker layer shall output more force (increased stiffness) while a thinner layer shall output more strain under the same electric field density. As stated by the supplier the maximum strain is 3.5% under an electric field of 100V/µm, see figure 3.2[62]. A thickness of $8\mu m$ was chosen for the P(VDF-TrFE-CTFE) layer.

The thickness of the substrate can be chosen by the specifications the designer prefers, for this thesis 50 µm Kapton was chosen. Kapton is an insulating polymer with high stiffness, this material is widely available and can be easily processed. Kapton can be cut using a laser cutter or scissors. The choice of this material was made because Kapton is the main substrate material of choice for flexible electronics and would, therefore, give a nice starting point for future applications.
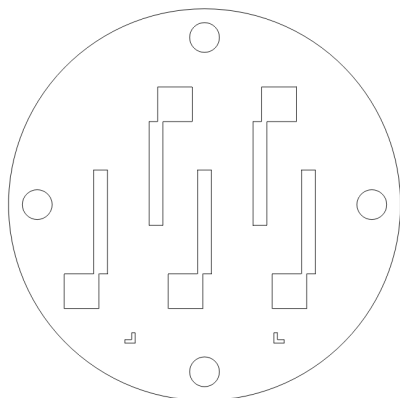
Figure 3.3: Example mask design. The samples are spread in the center, the alignment features are in the lower region in the form of corner-L shape and the connection holes are spread around the circle to ensure tight connection during sputtering.

3.3. Mask Design

For mask design, certain points have to be considered. Mask size, Spacing between samples, alignment features and connection holes.

The mask size is decided by the smallest machine chamber in the process, in our case the sputter coater. There are two sputter coaters at 3ME, "ATC Sputter deposition chamber" and the "Quorum mini SC7620". The Quorum can handle masks with a maximum size of $\varnothing 60mm$ and the ATC can handle samples with a maximum size of 300mm. The operation of the Quorum mini sputter coater is much easier w.r.t. the ATC, the quorum is currently also the only system in a cleanroom making this the only choice for the project.

The Spacing between the samples should be chosen according to the cutting step in the production process. If the laser cutter is used, gaps of more than $0.2mm$ should be ensured to keep enough space to align and cut out the samples. An example of one of the masks is displayed in figure 3.3, the masks in this project are made with a larger spacing since the initial choice for the cutting step was to cut out the sample with scissors. This was not the best choice and therefore switched to cut out the samples using the laser cutter.

The alignment of the samples is important for single layer samples and of very high importance for multilayer samples. When the layers are not perfectly aligned, the electric field density over the polymer might not be constant and the cutting step can be tedious, increasing the chance of failure. The alignment features in the sample mask are L-shapes, these features give good alignment in x- and y-direction. The use of two alignment features enables the possibility of aligning the mask in rotation around the z-axis.

The connection holes make sure the mask and the samples are kept aligned and more importantly that there is a tight parallel connection between the mask and the sample. If the mask or sample would not be flat (within certain bounds) there would be a gap between the two, the electrodes sputtered would not be neatly defined by the shape of the mask.

4

Dynamics & Control

The model used to predict the actuators behaviour is based on the book "Piezoelectric Multilayer Beam Bending Actuators" [36]. While the actuator in this thesis has only one active layer, a monomorph, this model can be used for multiple active polymer layers. The model was initially derived for ceramic piezoelectric materials, by changing the electromechanical and material specific parameters, the model can also be used for relaxor-ferroelectric polymers.

4.1. Theoretical Dynamic Model

The final model in the form of a transfer function is equation 4.1, where ζ is deflection, u_{piezo} is input voltage, Y is the gyrator constant(equation 4.16), n_m is the reference compliance (equation 4.18), X_m the eigenmode of m (equation 4.17), ω the input frequency, ω_m the specific eigenfrequency m (equation 4.13) and Q_m the damping ratio (equation 4.19). How this model is derived is described in great detail in the reference book[36], this chapter only explains the components that are used for actuation part of the derivation.

$$\frac{\xi}{u_{piezo}} = \frac{1}{Y} \sum_{m=1}^{\infty} \frac{n_m X_m(l) X_m(l)}{[1 - (\frac{\omega}{\omega_m})^2 + j \frac{\omega}{\omega_m} \frac{1}{Q_m}]} \tag{4.1}$$

To implement and analyse the model Matalab was used, the full code can be found in appendix A. With this model figure 4.1 is created, the blue line corresponds to the model. From this model, where the design specifications from chapter 3 are implemented, we can depict two important parameters, the stiffness line at -150dB and the first eigenmodes at $60Hz$ an $400Hz$. These parameters are from importance in the design of a controller in section 4.3.

The electromechanical components of the model are based on the thermodynamic equation 4.2 which states the internal energy density of a volume. If we take the partial derivative of this equation and we keep the temperature Θ and the entropy Σ constant we find the piezoelectric equations 4.3 and 4.4. Where ε is the permittivity, d_{ikl} is the piezoelectric coefficient and s_{ijkl} is the elastic coefficient. The final total energy density is displayed in equation 4.5.

$$dU = \Theta d\Sigma + T_{ij} dS_{ij} + E_i dD_i \tag{4.2}$$

$$D_i = \varepsilon_{ik}^T E_k + d_{ikl} T_{kl} \tag{4.3}$$

$$S_{ij} = d_{ijk} E_k + s_{ijkl}^E T_{kl} \tag{4.4}$$

$$w_{tot} = \frac{1}{2} E_i D_i + \frac{1}{2} T_{ij} S_{ij} \tag{4.5}$$

The total flexural rigidity and internal piezoelectric moment can be calculated by taking the Bernoulli beam bending theory. The flexural rigidity C can be calculated with equation 4.6. Where w_i is the width of the layer, S_{11}^E is the elastic compliance at a constant electric field, h_i is the thickness of layer i and $\bar{z}$ is the
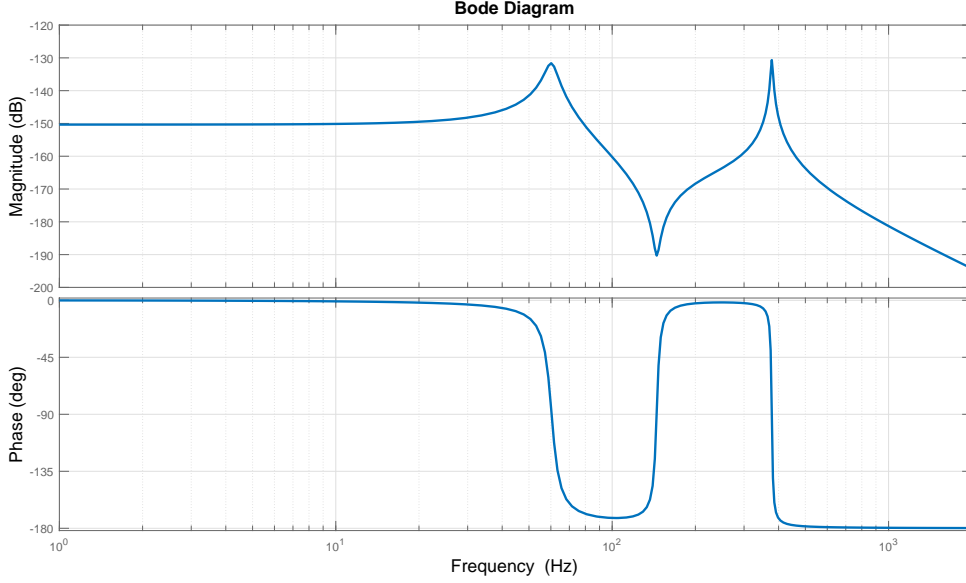
15

Figure 4.1: Bode plot of the ferroelectric model. On the vertical axis is displayed the deflection in µm (dB scale) and on the horizontal plot the input frequency in Hz. The peaks represent the resonance peaks on the eigenfrequency ω_m.

neutral axis position (equation 4.9). This equation is formulated using the full range of layers from layer 1 to i. The piezoelectric moment m_{piezo} is defined as equation 4.7.

$$C = \frac{1}{3} \sum_{i=1}^{n} \frac{w_i}{s_{11,i}^E} \left[3h_i \left(\bar{z} - \sum_{j=1}^{i} h_j \right) \left(\bar{z} - \sum_{j=1}^{i-1} h_j \right) + h_i^3 \right] \tag{4.6}$$

$$m_{piezo} = \frac{1}{2} \sum_{i=1}^{n} \frac{w_i d_{31,i}}{s_{11,i}^E h_i} \left[2\bar{z}h_i - 2h_i \sum_{j=1}^{i} h_j + h_i^2 \right] \tag{4.7}$$

Combining this equation with the try function for estimating cantilever beams, we can find the deflection of the total cantilever with equation 4.8. M is the bending moment, U the applied voltage, x the position on the cantilever and l the total length.

$$\xi(x) = M \frac{l^2}{2C} \left(\frac{x}{l} \right)^2 + U \frac{m_{piezo} l^2}{2C} \left(\frac{x}{l} \right)^2 \tag{4.8}$$

The dynamics of a cantilever are based on Bernoulli Hypothesis of beam bending theory [63]. Because of the a-symmetric geometry of the cantilever over the x-axis, figure 4.2, it is important to find the neutral axis position, this is calculated with equation 4.9. The range in the summation is from 1 to 2 since there are only two layers present that contribute to the thickness of the cantilever.

$$\bar{z} = - \frac{\sum_{i=1}^{2} \frac{w_i}{s_{11,i}} h_i^2 - 2 \sum_{i=1}^{2} \frac{w_i}{s_{11,i}} h_i - \sum_{j=1}^{2} h_j}{2 \sum_{i=1}^{2} \frac{w_i}{s_{11,i}} h_i} \tag{4.9}$$

Disregarding the derivations made to get here, see reference [36], we continue with the differential equation 4.10 for piezoelectric actuators. To find a transfer function that can serve as a model we start with a generalized eigenvalue problem 4.11. The eigenmode X can be calculated with equation 4.17, which uses the Rayleigh functions and the wave number k to find a solution. With the correct boundary conditions each individual wave number k_m can be solved with equation 4.12, the solutions as a result of numerical analysis are listed in table 4.1. The eigenfrequency can now be calculated with equation 4.13. Where l is the length of the cantilever, $/mu$ is the mass per unit length, E is the Young's modulus, I is the moment of inertia and m is the total mass.

Table 4.1: Numerical solutions of the characteristic equation 4.12.

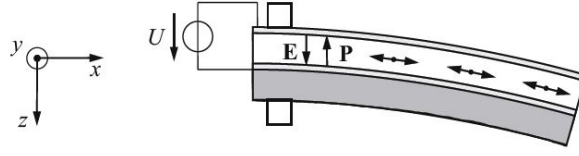| m	1	2	3	4	5	...
k_m l	1.8751	4.6941	7.8548	10.9955	14.137	...

Figure 4.2: Deflection of actuator by strain in the piezoelectric material as a result of the electric field E.

$$\frac{C\partial^4 \xi(x,t)}{\partial x^4} + \mu\frac{\partial^2 \xi(x,t)}{\partial t^2} + r_a\frac{\partial \xi}{\partial t} = f(x,t) \tag{4.10}$$

$$\xi_h(x,t) = X(x)\phi(t) = X(x)\phi_0 e^{j\omega t} \tag{4.11}$$

$$1 + cos(k_m l)cosh(k_m l) = 0 \tag{4.12}$$

$$\omega_m = \frac{k_{ml}^2}{l^2}\sqrt{\frac{C}{\mu}} = \frac{k_{ml}^2}{l^2}\sqrt{\frac{EI}{m}} \tag{4.13}$$

When the eigenmodes and eigenfrequencies are known the frequency response can be calculated, the extend of this calculation is based on the amount of eigenmodes added in the equation 4.14. This is according the superposition principle and is extensively reported by M. Abu-Hilal[64].

$$\xi(x,t) = \sum_{m=1}^{\infty} X_m(x)\phi(t) \tag{4.14}$$

To ensure that the time dependent behaviour of the eigenmodes can be calculated individually at any point x on the beam, it is important to ensure the orthogonality conditions of the eigenvalue problem. The orthogonality conditions can be confirmed with equation 4.15.

$$X_m \cdot X_n' = 0, m \neq n \tag{4.15}$$

To find the electromechanical component in the transfer function we consider the gyrator constant $1/Y$. To find this constant we take a look at figure 4.2, the derivations made are under the constraint of assuming only strain in the x-direction as a result of voltage u over the electrodes. Starting with equation 4.3, we acquire equation 4.16, where h is the thickness of each individual layer, w is the width of the layer, s_{11} is the elastic compliance and d_{31} is the piezoelectric constant. We sum from one to two since we only have two layers, a substrate and an active piezoelectric layer. Note that the d_{31} of the substrate is much greater than from the active polymer layer.

$$\frac{1}{Y} = -\sum_{i=1}^{2} \frac{w_i d_{31,i}(h_{o,i}^2 - h_{u,i}^2)}{2s_{11,i}^E h_i} \tag{4.16}$$

$$X_m(x) = \tilde{c}(k_{mx}) - \tilde{s}(k_{mx})\frac{\tilde{C}(k_{ml})}{\tilde{S}(k_{ml})} \tag{4.17}$$

$$n_m = \frac{4n_0}{(k_{ml})^4} \tag{4.18}$$

$$\frac{1}{Q} = \frac{rl}{k_{ml}^2}\sqrt{\frac{1}{C\mu}} \tag{4.19}$$

Table 4.2: Solution of the characteristic equation $1 + cos(kl)cosh(kl) = 0$[36]. Each wave number k_m can be used to find the individual eigenfrequencys with equation 4.13.

m	1	2	3	4	5	...
$k_m l$	1.8751	4.6941	7.8548	10.9955	14.137	...

4.2. Model verification

To verify the model composed in section 4 a model verification process was performed. By fitting experimentally obtained bodeplots to the theoretical model it will be verified that the theoretical model is correct. To find the bode plot of the individual actuators, Matlab's tfestimate() function is used. Tfestimate estimates a transferfunction given an input signal, x, and an output signal, y. By dividing the input and output signals into pieces the function is repeated several times and an average is given as output, this is done with the window variable. The sample frequence is specified in Fs and the frequency range can be set with f.

$$[txy, f] = tfestimate(x, y, window, noverlap, f, Fs) \tag{4.20}$$

What tfestimate does is divide the cross power spectral density of the in and output with the power spectral density of the input, equation 4.21. The power spectral density can be calculated using Fourier analysis[65].

$$H(f) = \frac{P_{xy}}{P_{xx}} \tag{4.21}$$

The input of this system can be anything, as long as the frequency's that are calculated in the tfestimate are all presented. A multi-sine can give a nice result, instead the iddata() function from Matlab was used. This function generates a signal within the set frequency range in the variable, $Frequency$. The input is specified as u the output as y and the sample time is set with Ts.

$$data = iddata(y, u, Ts, 'Frequency') \tag{4.22}$$

4.3. Control scheme

When designing a controller it is important to set boundary conditions. What is the target motion and in which frequency range should the actuator perform. Two examples of applications can be a hexapod crawling robot[66] or the stiffness control for the wings of a flying robot[67]. For a walking robot using these cantilever type legs, actuation in the first eigenfrequency would be the best solution. When actuating in the eigenfrequency range the amplification factor Q, equation 4.19 can be multiplied to the base stiffness line of the dynamic model. The combination of the maximum displacement of the actuator with a high frequency results in a fast walking robot. For the stiffness control of butterfly wings a quick step response is preferred. In this section, an example controller for such a butterfly wing is designed.

By analysing the model in chapter 4, figure 4.1 we can design a controller. From this figure the eigenmodes and stiffness line can be depicted, the first two eigenmodes at 60 and 400 Hz stand out over the stiffness line. The resonance of these eigenmode cause oscillations when controlling in the lower frequency ranges. To remove this characteristic a feedforward controller is designed using the pole-cancellation method. The idea of pole cancellation is to get rid of the two peaks and increase the phase so that is would stay above -180 deg in the controllable region. To accomplish this a notch filter and a low pass filter can be used on the first peak, this will completely remove the first peak while suppressing the second peak below the stiffness line. A notch filter is basically the inverted model multiplied with some poles to make the controller realistic. If these poles are not added the filter would have infinite gain and that is physically hard to realise. Since the notch filter is an inverted model, the factor ζ is $1/2Q$ where Q is defined in equation 4.19. The transfer function of the notch filter is described in equation 4.23 and the low pass filter in equation 4.24. Combining both would result in equation 4.25.

$$C_{notch} = \frac{s^2 + 2\zeta_0\omega_0 s + \omega_0^2}{s^2 + 2\omega_0 s + \omega_0^2} = \frac{s^2 + 2\zeta_0 2\pi f_0 s + 2\pi f_0^2}{s^2 + 2 \cdot 2\pi f_0 s + 2\pi f^2} \tag{4.23}$$

$$C_{lowpass} = \frac{\omega_0}{s + \omega_0} = \frac{1}{\frac{s}{2\pi f_0} + 1} \tag{4.24}$$

$$C = \frac{s^2 + 2\zeta_0\omega_0 s + \omega_0^2}{(s+\omega_0)(s^2 + 2\omega_0 s + \omega_0^2)} = \frac{s^2 + 2\zeta_0 2\pi f_0 s + 2\pi f_0^2}{(\frac{s}{2\pi f_0} + 1)(s^2 + 2\cdot 2\pi f_0 s + 2\pi f^2)} \tag{4.25}$$
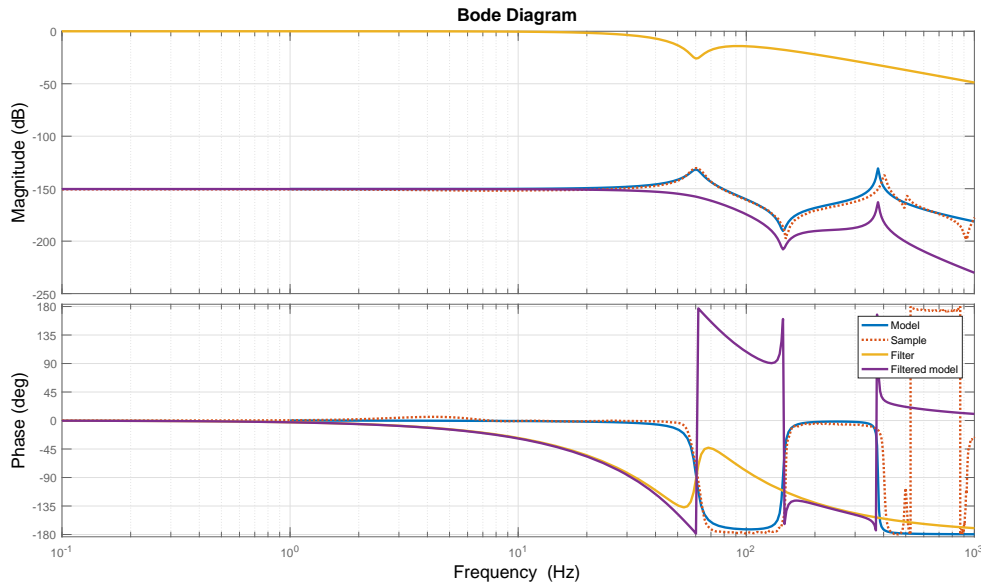

Figure 4.3: Bode plot of the controlled model. Displayed in blue is the theoretical model, in red is the measured system, in yellow the notch and low-pass filter combined and in purple is the controlled model.

The Bode plot in figure 4.3 displays the model (Blue), the filter (Yellow) and the feedforward controlled model (Purple). As can be seen the resonance peaks in the controlled model are now all below the stiffness line and the sample can be controlled up to 60 Hz. At 60 Hz the phase drops below -180 deg and the system would become unstable. A block wave input simulation and corresponding measurement is displayed in figure 4.4. As can be seen in the figures 4.4 the simulation is not spot on with the measured data, the measured data damps out the resonance significantly but not so much as in the simulation. in the second step of figure 4.4b there is a slight resonance of 10Hz, the origin of these vibration might be to the disturbance of the piezo-electric response. In figure 4.5 a triangular input signal is transformed to a m-shape, this happens because of the unidirectional response of the piezoelectric material in α-phase, see section . A full polarised sample would follow the triangular input better. If this effect is disregarded the resonance is damped out completely and the signal is tracked without oscillations.

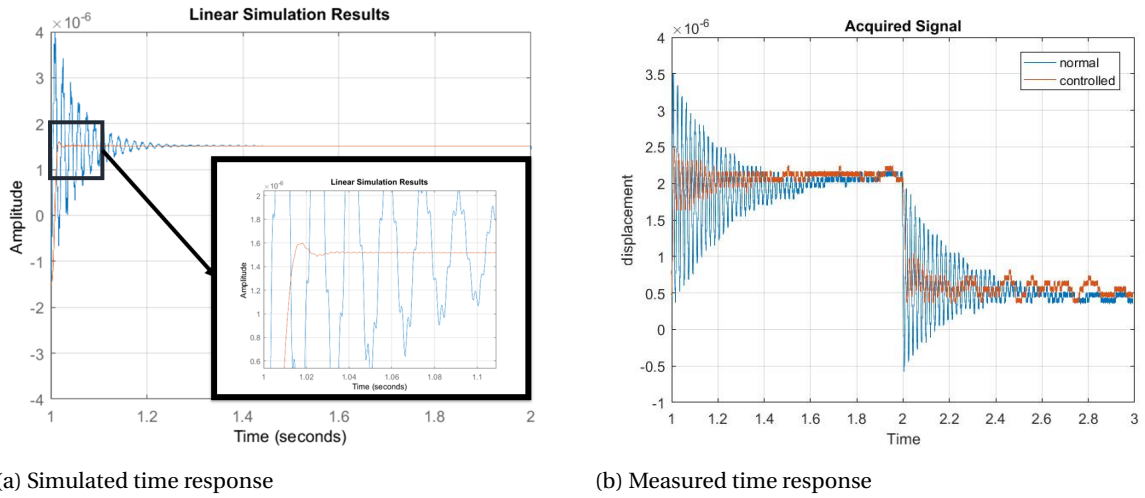(a) Simulated time response

(b) Measured time response

Figure 4.4: Time response of piezoelectric model with a blockwave input signal. Subfigure (a) illustrates the simulated response with in blue the uncontrolled model and in orange the controlled model. Subfigure (b) illustrates the measured cantilever, in blue the uncontrolled sample and in orange the sample with a controller.
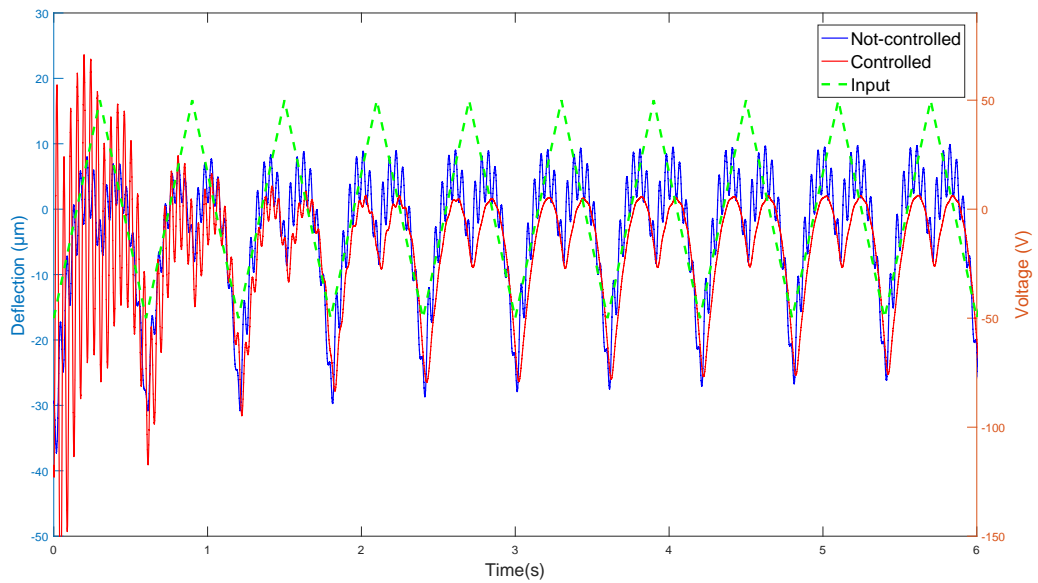

Figure 4.5: Time response of piezoelectric model with a triangle input signal. The data in blue represent the not controlled response, the red lines represent the controlled response and in green the triangular input signal. Observe that the first three periods the material is still setling to the voltage values.

<div align="right">

5

</div>

<div align="right">

Methods

</div>

The key to production of actuators is working clean. A clean environment and properly cleaned products will ensure proper samples, dust particles will destroy the thin film capacitors. In this chapter all steps required to successfully produce relaxor-ferroelectric actuators shall be presented. Besides this chapter appendix B contains a step by step picture guided reference document.

5.1. Shadowmasks and Baseplate

To create both shadow masks and base plates, stainless steel sheets of 100μm are used and defined by laser etching/cutting equipment. For the samples in this thesis, an OPTEC 15W Talon UV laser was used to precisely (resolution up to 20μm) cut out the shadow mask design. The system settings used, to quickly cut through these sheets, are listed in Table 5.1.

5.2. Synthesizing Polymergel

P(VDF-TrFE-CTFE) powder (PVDF:TrFE:CTFE = 62:31:7 in mol%) was purchased from PIEZOTECH ARKEMA[68] and dissolved in 2-butanone (MEK) (ACS reagent, ≥ 99%, Sigma-Aldrich) at a concentration of 1:5. The solution was stirred extensively to ensure a proper consistency. Then the solution was set in a desiccator to remove all air bubbles. This is an important step, if there are bubbles in the polymer layer after spin casting the thin layer would have holes which in turn result in an electrical shortcut system in the actuator. An example of a hole is displayed in figure 5.1b.

Table 5.1: Settings OPTEC laser cutter

| Subject	Stainless steel	Polyimide
Thickness[μm]	100	50
Drill numbers[−]	4	2
Drilling step [mm]	0.015	0.015
number of levels[−]	4	2
Z-step [mm]	0.025	0.025
speed [$\mathrm{mm\,s^{-1}}$]	200	200
Jump Speed [$\mathrm{mm\,s^{-1}}$]	200	200
Laser firing Rate[$\mathrm{kHz\,Hz^{-1}}$]	35	35
Laser Power [%]	100	30
Pulse per burst[−]	99	99
Burst time[μs]	1000	100
Repetitions[−]	160	20
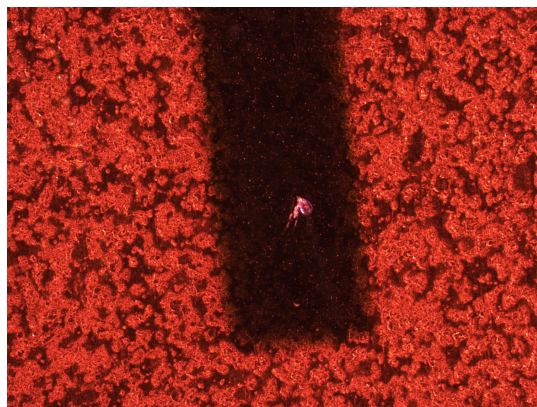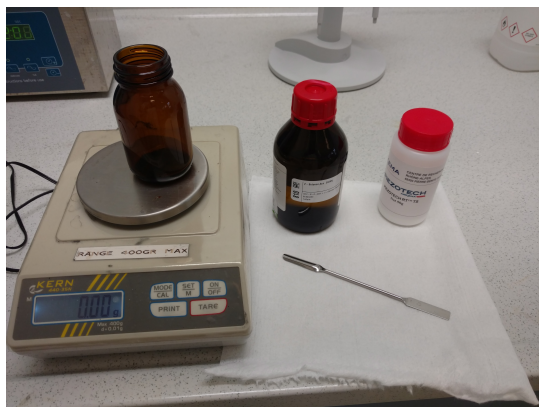
(a) Mix P(VDF-TrFE-CTFE) with 2-butanone with a ratio 5:1 (b) Hole as a result of bubbles in the gel solution, such a hole to create a polymer gel.   creates a short circuit between the two electrodes.

5.3. Attaching Substrate to Baseplate

To spin coat the P(VDF-TrFE-CTFE) on the flexible polyimide substrate a a rigid surface is needed, the baseplate ensures stiffness while spinning the polymer into an even layer. The connection between the substrate and the baseplate is to be stiff but should be easily removable. Spray adhesive 3M is used to make a rigid connection, this specific adhesive can be easily removed when the base plate is no longer needed.
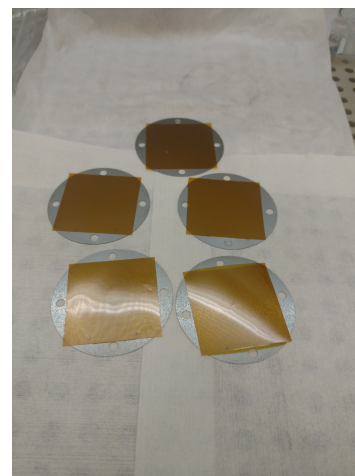
The adhesive can be removed using a acetone or MEK wetted scalpel and carefully slicing under the substrate surface. Make sure the adhesive layer is wet from the solvent to avoid reattachment while pulling away the polyimide substrate from the stainless steel backplate.
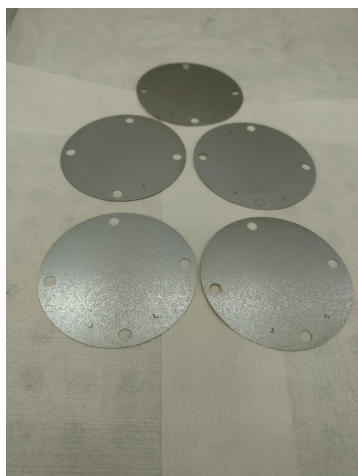
(a)   (b)   (c)

5.4. Alignment

To ensure that the capacitor electrodes are neatly aligned with each other, alignment features are cut in the masks and baseplate, see section 3.3. Using light and a magnifying glass these alignment features can be aligned with high accuracy, aligning translation in x- and y-direction and rotation around the z-axis. When the mask is aligned with the backplate use some nylon screws to connect the two together, pressing the mask to the sample and locking the alignment.

5.5. Electrodes

To define electrodes on the substrate and active polymer layers a sputter coater was used, an alternative would be aluminium evaporation or any other polymer metallization technique.

Connect the sample to a shadow mask using Nylon screws and bolts, ensure the alignment is perfect using
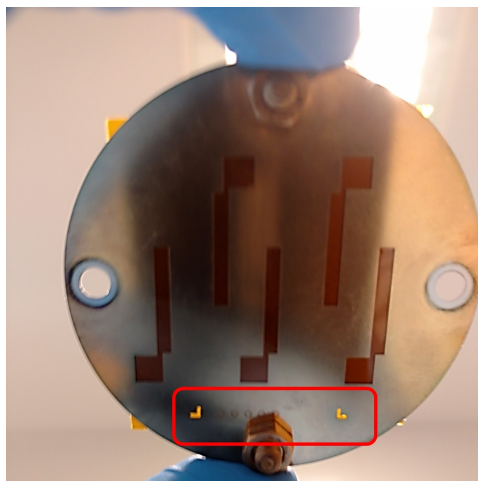
Figure 5.3: Alignment features used to align mask with baseplate to ensure the gold electrodes are aligned properly.

a magnifying glass and the alignment features discussed in section 5.4. If the alignment is not done correctly the electrodes might make contact and the electric field over the capacitor shall not be uniform.

Gold (Au) electrodes with a thickness of $40nm$ are formed by sputtering with 10mA at $0.1mbar$ vacuum for 8 minutes on the Emitech sputter coater. Alternatively $20nm$ layers can be sputtered using 25mA at $0.15mbar$. Always work with clean samples and a clean chamber, any dust particle can ruin the samples by causing a short-circuit between the electrodes.

When using the solvent annealing process (section 5.7), ensure the sputter coater is cooled after every use, temperature rises can influence the electromechanical response of the polymer and may even damage the machine.
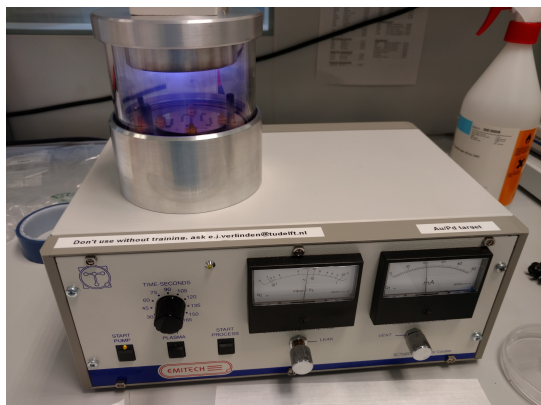
(a) Sputter coater used to sputter electrodes through the SS shadow mask.
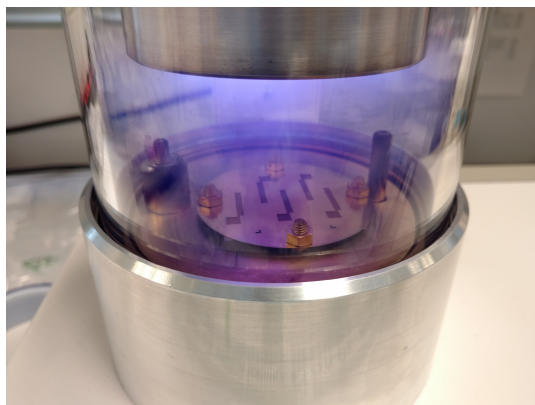
(b) Close up of plasma which sputters the electrodes on the polymer.

Figure 5.4

5.6. Thin Polymer Layer

To create a uniform layer of P(VDF-TrFE-CTFE) a spin casting method is used. First a droplet of MEK + P(VDF-TrFE-CTFE), 5:1, is deposited on the substrate, then a spin casting process is started. Rotation speed and spin duration influence the layer thickness off the polymer layer. In figure 5.5 the dependency of layer thickness as a result of spin casting speed can be seen, this was all done with a spin duration of 30 seconds. The measured result is a bit off since the initial volume poured on the substrate is also of importance in the final thickness of the polymer layer. The layer thickness relation can be calculated with equation 5.1 [69], where h is the layer thickness, μ is viscosity, t is spin cast time and η is spin cast speed. All the samples made in this research are created with 2000rpm spin speed, resulting in $8\mu m$ thick samples.
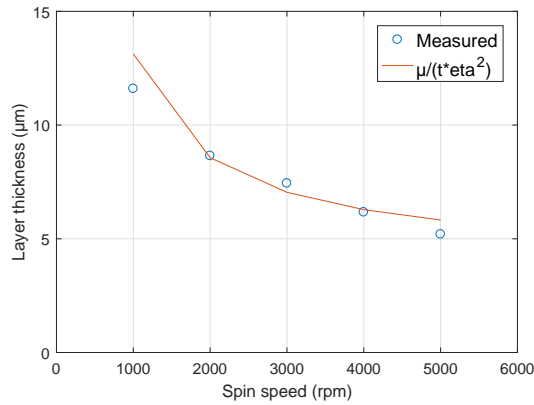
Figure 5.5: Polymer layer thickness as result of spin casting speed. Keeping the viscosity constant (polymergel 5:1 as presented in section 5.2) and spinning with $t = 30s$.

Table 5.2: Boiling point of mixed materials

	Boiling point
MEK	79.64°C
P(VDF-TrFE-CTFE)	122°C

$$h \propto \sqrt{\frac{\mu}{t\eta^2}} \tag{5.1}$$

5.7. Annealing

Annealing is an important step in creating electromechanical polymers. It enhances the polymerization process, creating long polymer chains and therefore increasing the electromechanical response. Annealing also has the purpose to remove residual stress and ensures proper connection to the substrate[2].

To anneal the polymer two different methods were used, temperature and solvent annealing. The most established method is temperature annealing, where a vacuum oven is used to ensure all the solvent evaporates from the polymer layer. To anneal the samples in a good fashion the boiling temperature of both the solvent and the P(VDF-TrFE-CTFE) should be considered, the specific boiling points are listed in Table 5.2. To stay below the boiling point of the required polymer and by the advice of the supplier, the annealing temperature of 111°C is chosen.

A second method which could be used is solvent annealing. With solvent annealing, a vapour of the same solvent used to dissolve the polymer in the first place, combined with time ensures the polymerisation. After this step, a vacuum chamber is used to remove the residual solvent in the material. The power of this step with respect to thermal annealing is to keep the sample at a low temperature all the time. The reason for this step was first stated in [16], by keeping the temperature of the polymer low the beta-phase (see section 2.4) of the polymer is maintained. Increasing the temperature over 50°C would result in more formation of alpha-phase and destruction of beta-phase, this process is illustrated in figure 5.6. As stated by Cho er al. [16] this process is irreversible, this measurement was repeated and indeed after a heating cycle, the material is irreversibly modified to a dominant alpha phase, see chapter 6.2.1.

5.8. Polarization

Polarisation can be done with many different methods, see Chapter 6.1.1. In this thesis two methods are used, initially, the focus is with traditional thermal polarisation. Thermal polarisation is the easier method, using a temperature component and a DC voltage on the samples the actuators would become polarised. An additional methods which was found during the work done in this thesis would be solvent polarisation. The basic setup is similar to thermal polarisation only the temperature component is replaced by a vapour of solvent, the same solvent used to dissolve the polymer in the first place.
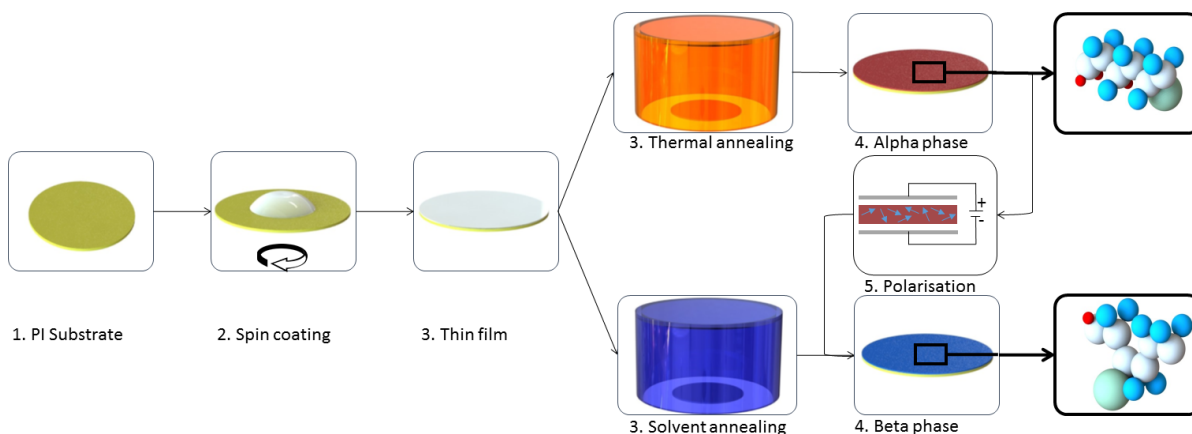
Figure 5.6: The influence of different annealing methods is dispalyed in this figure. As a result of thermal annealing α phase would be more present While solvent annealing would result in more β phase material. With an additional polarisation step the Beta phase can be attained again.

Thermal polarisation is done with a constant temperature of 85°C, this temperature was applied using an "IKA RH Basic" hot plate, a glass cover was used to maintain the heat. Voltage was varied between 60V-140V to measure the influence of electric field density on the polarisation effect. The polarisation time was set at 25 minutes. While multiple studies show that 1-5 minutes would be efficient [70][71], the risk of improper polarisation because of short periods should be avoided. Finally, there is a sample holder which connects the electrodes to a DC-Voltage source(a maximum of 140V was available for this research) through some wires which are clamped with nylon bolts. After 25 minutes the temperature should be lowered to room (operating) temp while the voltage is kept high. When room temperature is reached the voltage step can be removed. The final setup for polarisation can be observed in figure 5.7a.

Solvent polarisation is done with a similar setup. The glass container which is used in the previous setup to contain the heat is now used to contain the vapour. Under the sample, a glass container holding a solvent (in this research 2-butanone/MEK) is positioned. The sample holder is connected to the electrodes of the sample and a DC-voltage source. The same timestep as in the thermal annealing process is maintained to ensure stability and possibility to compare the two methods. The complete setup can is displayed in figure 5.7b.
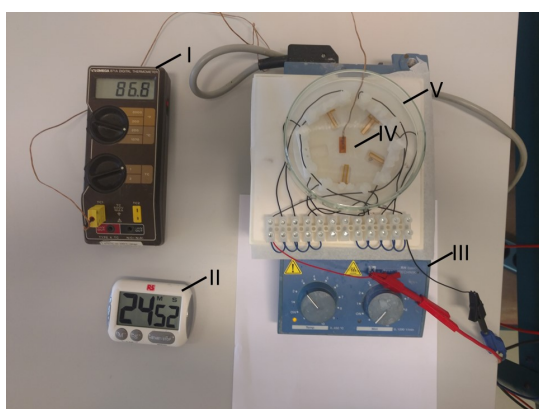
(a) Thermal polarisation setup. Displayed in this figure: I. Thermometer, II. timer, III. hotplate, IV. sample holder with samples and V. glass cover.
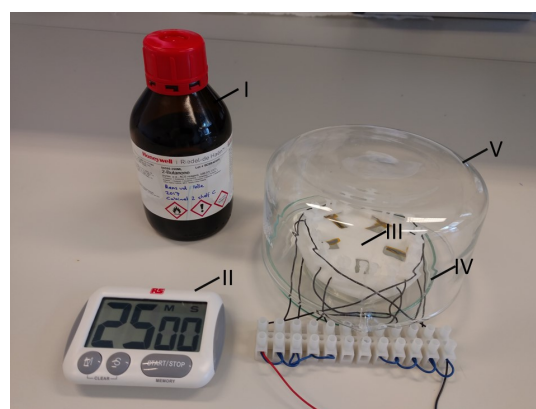
(b) Solvent polarisation setup. Displayed in this figure: I. Solvent (2-butanone), II. timer, III. sample holder with samples, IV. glass container with solvent and V. glass cover.

Figure 5.7

Table 5.3: Displacement decoder specifications adapted from the polytec manual [72].

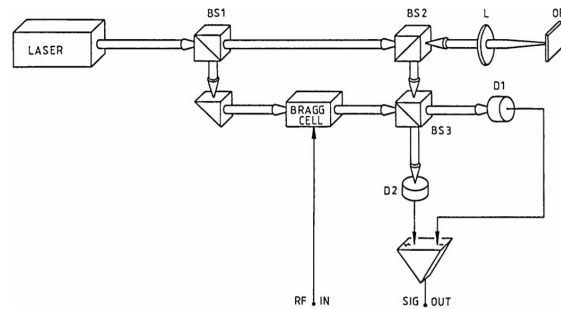| Measurement Range	Full Scale Output	Resolution	Max. vibration frequency	Max. velocity
$\mu m \, V^{-1}$	mm	μm	kHz	$m \, s^{-1}$
0.5	0.008	0.002	25	0.06
2	0.032	0.008	75	0.25
8	0.13	0.032	75	1.0
20	0.32	0.08	250	1.6
80	1.3	0.32	250	1.6

Figure 5.8: The Mach Zehnder Interferometer as the working principle of a laser vibrometer[72].

5.9. Verification

5.9.1. Laser Doppler Vibrometer

To measure deflection as a result of electrical input a Polytec OFV 505 single point laser Doppler vibrometer was used. positioning the sample 23cm from the vibrometer lens and aligning the system by rotating the sample until the reflected beam is centred on the lens enables fine measurement. With the single point system deflections in the nanometer range can bean measured with sampling rate up to 25kHz [72], see specifications listed in Table 5.3. These specifications make it perfectly suitable for this thesis, where deflections of $1 \mu m$ up to $300 \mu m$ are expected with the operating voltage from $1V$ to $200V$ and with a frequency range below 200Hz.

The laser Doppler vibrometer works with the principle of interferometry. The system measures the difference in the sinusoidal waves of the reflected beam. The complete mechanism of the polytec system is described in the reference manual [72], a schematic layout of the system is displayed in figure 5.8.

5.9.2. Data Acquisition

The measurement data from the laser Doppler vibrometer has to be gathered on the pc, this is accomplished using a data acquisition system from national instruments, NI-usb 6211. With either Labview, Python or Matlab this DAC can be controlled to manage in and output on the actuators. The in-/output of this system is $\pm$10V and can handle up to 250.000 samples per second. All the code that is used in Matlab to handle the system can be found in Appendix A.1.

5.9.3. X-Ray Defraction

Kepler [50] has shown that with x-ray defraction the polarisation process and its current state can be determined. He performed x-ray defraction measurement before and after polarisation and identified the change in crystal lattice orientation. He showed that the orientation of the orthorhombic crystal structure of PVDF can rotate freely about the polymer backchain. The corresponding peaks to the different phases in P(VDF-TrFE-CTFE) are found to be 18.4° for alpha-phase and 19.4° for the beta-phase [16].

The X-ray diffraction setup used is a Bruker-AXS D5005 diffractometer in Bragg-Brentano focusing geometry, equipped with a graphite monochromator in the diffracted beam. Cu Ka radiation. 45kV, 30 mA. Micrometer: 5.0. Slits: 0.6A16 / 0.6B16 / 6B16 / 0.6C16. The scan range in 2θ is from 10°-23° with step size of 0.03°, each step is measured for 4 seconds to achieve accuracy.

6

Results

The production of actuators was successful using the steps described in Chapter 5, in this section the verification measurements are presented. Next to the verification, some novel features that are discovered during the process are presented and implemented in the actuators. These features regard the solvent polarisation and annealing steps which prove useful in developing a stronger electromechanical response. Finally a step to remove residual strain in the active polymer layer which is induced by spin casting is presented.

6.1. Actuators

The produced actuators work and show electromechanical response as can be seen in the upper part of figure 6.1. The actuators output clearly shows a double sine wave, one following the input frequency and the other with double that frequency. These sine waves corresponding to the bidirectional piezoelectric response and the unidirectional electrostrictive response, also the beta- and alpha-phases. The response in strain from these different phases is graphically displayed in figure 6.2. The signals can be extracted forming two separate signals. This is done using a fast Fourier transform in Matlab, the found amplitude and frequency are used to build a new sine signal. The resulting signal is displayed in the lower part of figure 6.1.
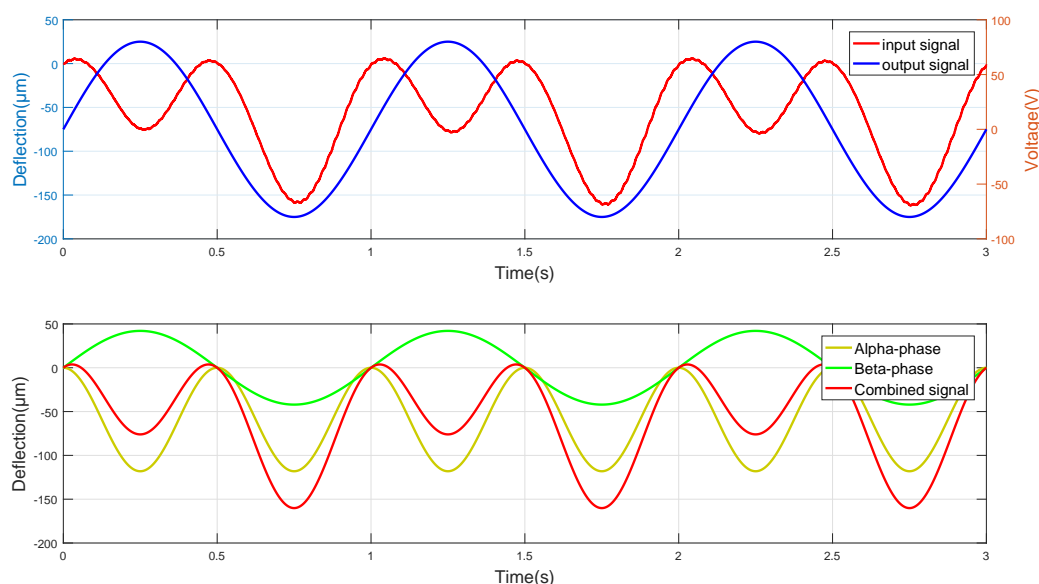

Figure 6.1: Measured deflection with a 160v sine wave at 1hz. In the upper figure the blue line represents the input signal while the red line represents the output signal, this is raw measurement data. On the lower image, the signal is decomposed with FFT and transformed in filtered response data. With in yellow the electrostrictive response, in green the piezoelectric response, and in red the combined signal again.
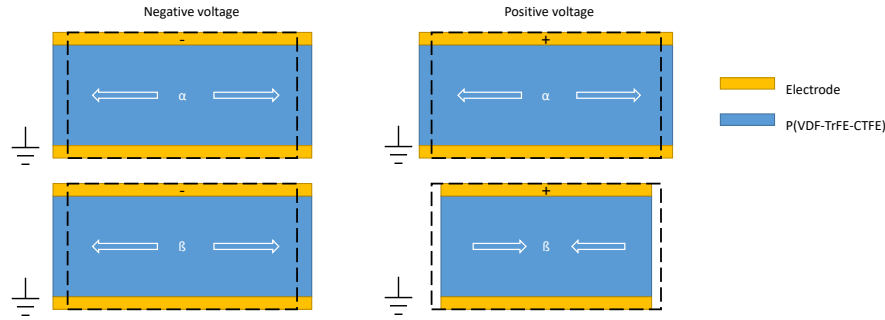
Figure 6.2: Strain induced by the different phases on P(VDF-TrFE-CTFE). On the left side there is a negative voltage on the top electrode, corresponding to both the α and β-phase to expand. On the right side there is a positive voltage on the top electrode, resulting in the α-phase part contracting while the β-phase expands again.
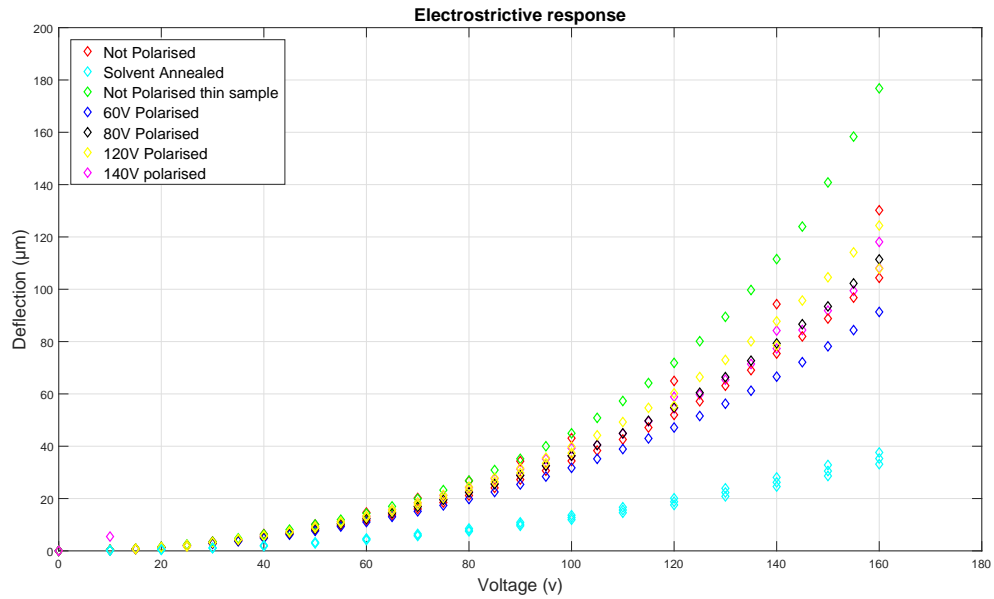

Figure 6.3: Filtered electrostrictive response of different samples on an increase of voltage with 1hz sine signal. The diamonds (◇) represent the electrostrictive response. The exponential electrostrictive response stays the same after polarisation.

6.1.1. Polarisation

Now it is established that there are two different output responses on a single input signal it is interesting to see how this material specific response can be used to the desired specifications of the designer. Measurements with different input voltage on different polarised sample have been performed, the result can be seen in figure 6.3 & 6.4. In these figures there is a considerable amount of information, the different colours and lines will be explained next. The exponential lines created by the circles in figure 6.3 represent the filtered electrostrictive electromechanical response. The linear lines formed by the small diamonds in figure 6.4 represent the piezoelectric electromechanical response.

The green colour represents a sample that has a slightly thinner active layer with respect to the other samples, The green data represent samples where the active layer is 4.3μm while all the other samples are 8μm. This sample is not polarised and the linear, piezoelectric response is almost zero. The electric field density, as a result of this thinner film, during operation is higher. Since the field density is higher the deflection increases. From this result,it can be stated that for maximum deflection, thinner films are more favourable. remember equation 6.1, the thicker film will result in higher stress and thus more strain and finally more blocking force. Blocking force has not been measured, this would be still an interesting topic to research in the future.

The purple colour matches samples which are polarised with 140V, it can be seen that they cross their
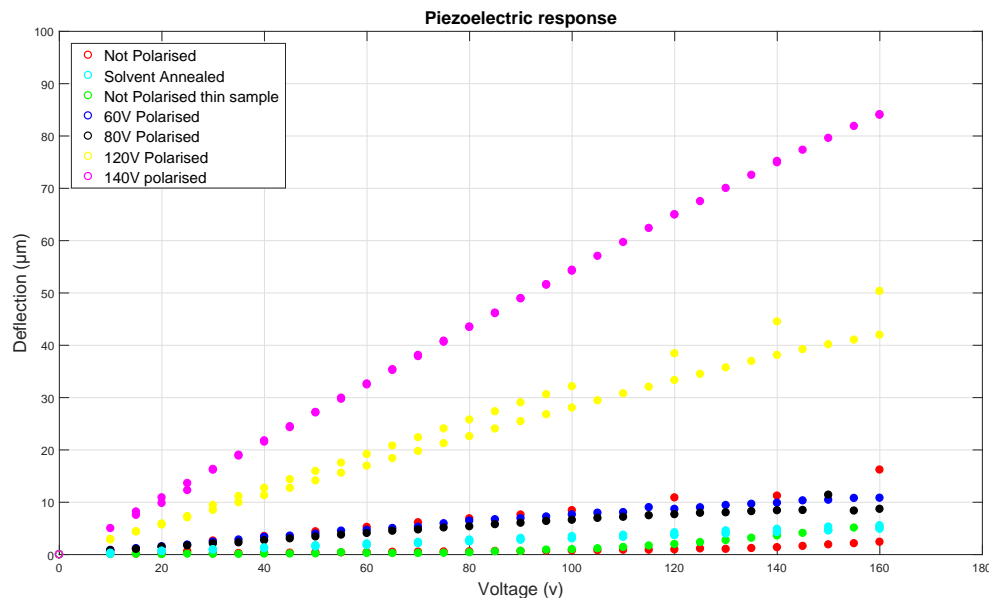
Figure 6.4: Filtered piezoelectric response of different samples on an increase of voltage with 1hz sine signal. The circles (o) represent the piezoelectric response. The linear piezoelectric response increases as a result from polarisation, formation of β-phase as a result from polarisation is shown.

piezoelectric counterpart around 130V. The yellow colour matches samples which are polarised with 120V, they cross their counterpart at 80V. The black colour matches samples which are polarised with 80V, they cross their counterpart at 30-40V. The blue colour matches samples which are polarised with 60V, they cross their counterpart at 30-40V. The cyan colour matches samples which are solvent annealed, they have much lower electrostrictive and piezoelectric response than their thermal annealed counterparts. It appears that after the polarisation voltage the linear piezoelectric part is dominated by the exponential electrostrictive part for each sample where a polarisation step is applied.

The deflection amplitude as a result of an input signal is the goal of an electromechanical polymer. The linear piezoelectric response increases with higher polarisation voltages. The slope of the piezoelectric response line appears to be doubled every time the polarisation voltage is increased by 20 Volt. While the piezoelectric response increased with polarisation, the electrostrictive response always remains the same disregarded of polarisation.

Next to the effect polarisation has on the maximum amplitude, the input to ouput direction is affected. When the sample is polarised in a certain direction the electromechanical response shall be stronger when the sample is actuated in the same direction. In figure 6.5 three figures represent this effect, in figure 6.5a the polarised sample is actuated with an input of $-30V$ to $30V$, figure 6.5b the same sample is actuated with an input of $-30V$ to 0 and in figure 6.5b the same sample is actuated with an input of $0V$ to 30. The difference between figure 6.5b and 6.5c is clearly in the fact that the electromechanical response for 6.5c is a lot stronger, the deflection in the positive input direction is significantly larger than from its negative input counterpart, see section 2.3. If a sample is polarised with a field direction upwards across it, for maximal electromechanical response it should be actuated with the same field direction.

6.1.2. Hysteresis
To measure the hysteresis a 10hz sine wave input with 200V potential was measured on a non-polarised and 140V temperature polarised polymer sample. The amplitude increase from a polarised sample is clearly visible from the image. The deflection in the non polarised sample is 100μm (=0.07% strain) while the polarised sample is around 290μm (=0.19% strain), using equations (6.2 - 6.3) the strain can be calculated. It can also be noted that the preference voltage at the polarised sample is negative, this is corresponding to the polarisation direction in which the sample is polarised. This preference voltage is not noticeable at the unpolarised sample.

The cause of the hysteresis is found in the viscoelastic material properties of the polymer. The internal
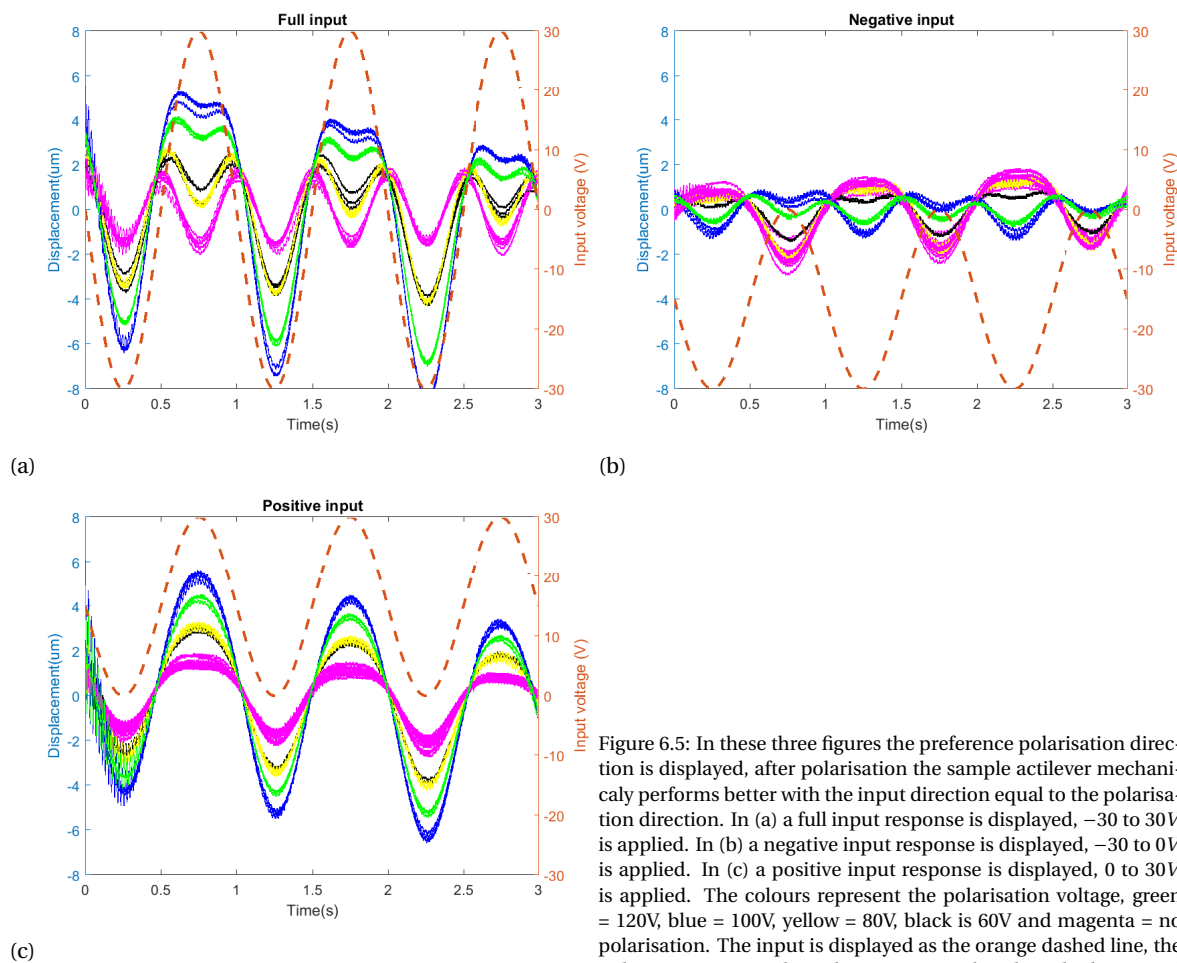
(a)

(b)

(c)

Figure 6.5: In these three figures the preference polarisation direction is displayed, after polarisation the sample actilever mechanically performs better with the input direction equal to the polarisation direction. In (a) a full input response is displayed, -30 to $30V$ is applied. In (b) a negative input response is displayed, -30 to $0V$ is applied. In (c) a positive input response is displayed, 0 to $30V$ is applied. The colours represent the polarisation voltage, green = 120V, blue = 100V, yellow = 80V, black is 60V and magenta = no polarisation. The input is displayed as the orange dashed line, the right axis corresponds to this input. Displayed on the horizontal axis is the time $0-3$ sec.

structure of the material is active, most of the reorientation in the molecular chain is transferred to electrical energy, the rest to heat, this is called dielectric heating. Since the strain-electric field ratio is high, the hysteresis is low. comparing the hysteresis this to the hysteresis strain of traditional PVDF, figure 6.7, it can be immediately noticed that the hysteresis is reduced significantly when the same strain is achieved.

6.2. Solvent annealing

6.2.1. X-ray defraction
Cho et al [16] reported that by heating a P(VDF-TrFE-CTFE) sample, the ferroelectric beta-phase is irreversible transformed into a full paraelectric alpha-phase. The same measurements are performed in this thesis and the result can be confirmed. Figure 6.8 displays the X-ray diffraction patterns with increasing temperature. Peaks at 18.4° 2θ represent the presence of alpha-phase, while peaks at 19.4 2θ represent the beta-phase. On the xy-plane, the centre of the peak is displayed. While increasing the temperature the concentration of the peaks shifts more to the left, even after cooling down the peak stay with a preference to the left half. While this image may not be as defined as in the research from Cho et al, the same trend is observable.

6.2.2. Mechanical deflection
The results from section 6.2.1 coincide with Cho et al's [16] paper. In their research, there was no effort done in electromechanical response of actuator systems. In figure 6.9b, the electromechanical response of a thermal and solvent annealed cantilever is displayed. While the thermal annealed system shows a full electrostrictive response on 2Hz, the solvent annealed system shows a combined 1Hz & 2Hz response signal. This might imply that the piezoelectric (beta) phase is stronger in the solvent annealed samples.

(a) Hysteresis of a non polarised sample.

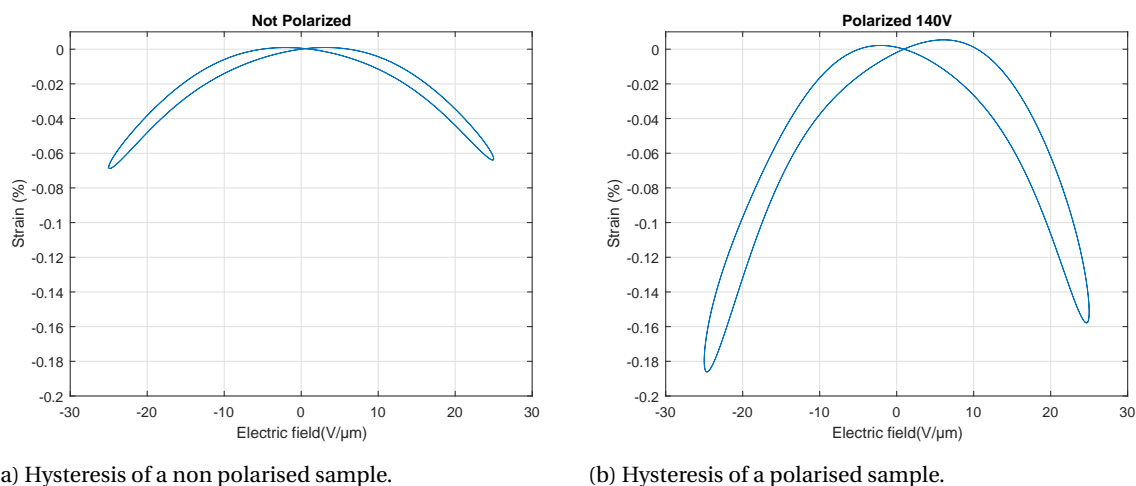(b) Hysteresis of a polarised sample.

Figure 6.6: Hysteresis of polarised and non-polarised polymer samples. The measured deflection is transformed to strain using equation 6.2 - 6.3.
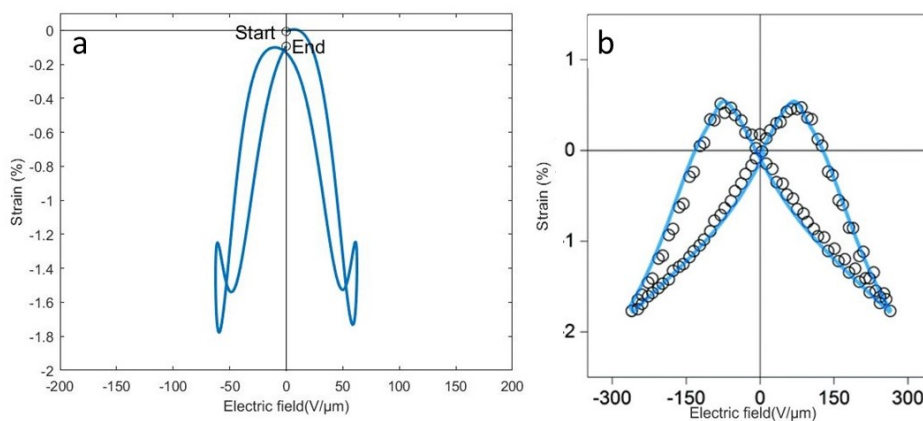

Figure 6.7: Hysteresis of polarised sample to compare with traditional PVDF. a) Polarized sample, 500V input voltage on 10Hz. b) Ferroelectric hysteresis and piezoelectric strain in solid-state pressed PVDF films. Measured (black) and modelled (blue) strain curves, measured vs. electric field[61].

Figure 6.9a displays the fast Fourier transform of the measured data, here the difference between the two sets become more clear. The thermally annealed set (red) show a very high 2Hz response w.r.t to the 1Hz response. This 2Hz response is directly related with the uni-directional response of a ferroelectric system. The solvent annealed set (blue) displays an even response in both the 1 and 2 Hz (uni- and bi-directional), implying that both piezoelectric and electrostrictive responses are evenly present. The results from figure 6.9 imply that the piezoelectric β-phase from solvent annealed samples are even stronger than from the thermally annealed samples. These measurement confirms the research performed by Cho et al [16] and prove that it can also be applied for electromechanical actuation.
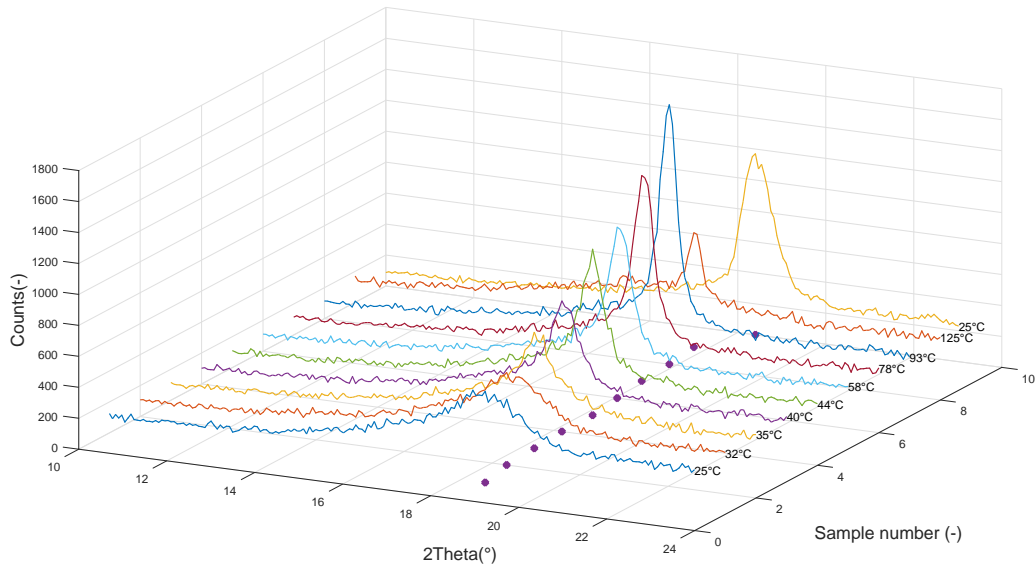
Figure 6.8: X-ray defraction pattern of thermally anealed samples which are heated from 25°C to 130°C and back to 25°C. In the vertical axis is the X-ray intensity, this corresponds to the amount of received X-ray data which is again dependend on the system settings and sample thickness. The height of the peak is not of great importance, the position and the height to width ratio are. on the x-axis is the 2θ reflection angle. The z-axis is only used to display the number of different samples in order from heating to cooling. On the xy-plane purple dots are displayed which represend the center of the measured peak. Note that above the melting temperature, 111°C the x-ray peak clearly collapses.

6.3. Solvent Polarisation

6.3.1. Results

The set of samples which are polarised with a solvent polarisation step are measured and compared to non-polarised samples. By comparing both sets it becomes clear that solvent polarisation is indeed a method to polarise ferroelectric polymers. The solvent vapour softens the polymer, when the polymer is softened an electric field shall rotate the polymer chain in a preference state.

In figure 6.10 the increase of electromechanical response as a result of polarisation is displayed. The magnitude of the electrostrictive response is 0.2µm both before and after polarisation. The magnitude of the piezoelectric response starts at zero before polarisation and ends with 0.3 µm after polarisation. This can imply a polarisation as a result of the flow of free hydrogen and fluoride atoms in the polymer while it is in a semi-liquid phase. Curing of the material using a vacuum system encapsulates the atoms in place resulting in a piezoelectric polarised material. This sine wave was created using a 30-volt 1hz source.

6.4. Solvent annealing to remove residual stress after spin casting

6.4.1. results

High-speed rotation of the spin caster acts as an evaporation step comparable to the temperature or vacuum annealing methods[73][26]. This sudden evaporation of solvent could be the cause of high internal stress in the active polymer layer. This so-called residual stress has a negative impact on the final form of cantilever shape actuators. Initial design alterations can be taken to counteract the deformation as a result of this residual stress. A method to (partly) remove this residual stress and counter bending of cantilever actuator would be more beneficial.

The amount of residual stress in a thin polymer film is a result of evaporation, also the processing techniques have influence on the residual stress. Injection molding, thermoset curing, electrochemical oxidation, plasma polymerization, laser ablation, pulse laser deposition, deposition-polymerization and spin casting are methods which can be used to create polymer films. Spin casting is the most widely common used method and this method is also used in this thesis. Several studies note that residual stress as a result of spin casting is a main factor for the dewetting of thin films[26][74].
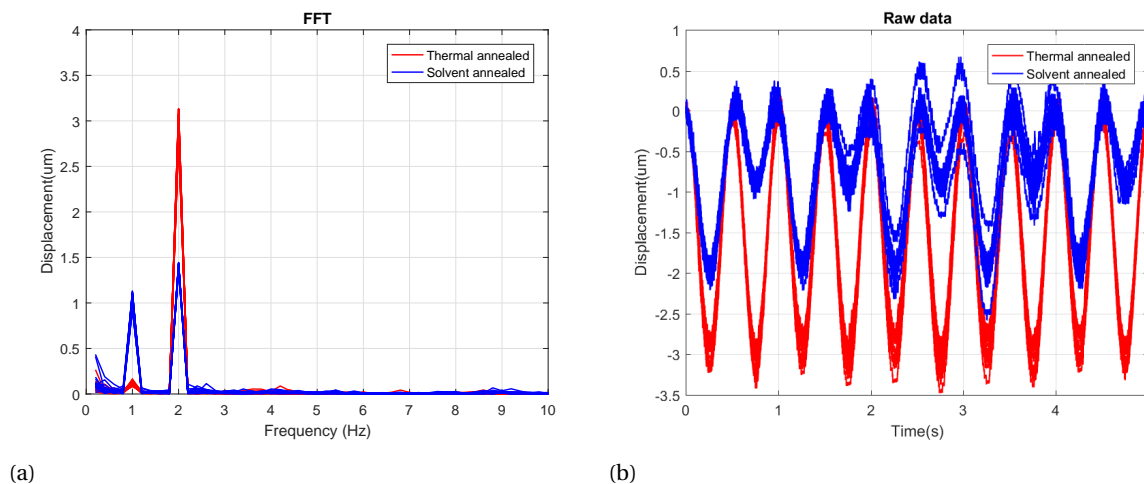
(a) (b)

Figure 6.9: Displayed on the left is raw data of input response of a 30 Volt sine wave at 1 hz. In Red there are 5 samples displayed which are thermally annealed while in blue there are 5 samples which are solvent annealed. On the right is FFT data of input response of a 30 Volt sine wave at 1 hz. In Red are 5 samples displayed that are thermally annealed while in blue are 5 samples that are solvent annealed.

While the polymer/solvent solution is spin casted, dry air flowing along the surface forces the polymer solution to evaporate rather quickly. The evaporation rate is defined by the temperature specific solvent/polymer combination and continues until a critical weight fraction is attained. When this concentration is reached the polymer turns to the glass state, it turns solid. While this is happening the polymer no longer flows but shrinks instead, residual stress is a result of the shrinking film and the forces between the film and the substrate. McKenna[75] has written a nice report with an example of polystyrene mixed with toluene. This material has shown to shrink approximately 14% in the glass state. This 14% shrinkage can be compared to a sudden increase of volume as an increase of temperature by $1400°C^{-1}$, the thermal expansion coefficient of $1e-4°C^{-1}$ will cause a volume change of 14%.

In figure 6.11a, a set of samples made with traditional spin casting and temperature annealing steps is displayed. Figure 6.11b, a set of samples which has been treated with a solvent annealing step is displayed. As can be seen clearly the right set has straight cantilevers compared to the left set. This was achieved by removing the residual stress with a solvent annealing treatment.

After the completion of the spin casting step, samples are set in a solvent annealing setup as shown in Fig 6.11. This setup consists of a locally contained vapour of the solvent used to dissolve the active polymer. This can be achieved with different methods, in this setup, a petri-dish filled with 2-butanone was covered with a large glass bowl. The sample was located on a smaller glass petri-dish turned upside-down in the first larger petri-dish, see figure 6.12. An alternative way is to use cloth soaked in solvent as a solvent-vapour source. Put these soaked cloths in the glass bowl and let the vapour evaporate. For both methods, it is wise to ensure the largest glass cover has a small opening at the bottom to let the heavier oxygen and Nitrogen float away while the lighter solvent fills the chamber.

6.4.2. Residual strain calculations
The strain in the active polymer layer can be calculated with equation 6.1[76]. Where σ is stress, E is the Young's modulus, d is the dielectric constant, R is the Radius (equation 6.2) and v is the Poisson's ratio. the subscript 1 and 2 refer to the layer where 1 is the P(VDF-TrFE-CTFE) layer and 2 is the substrate layer of the cantilever. When the stress is known the strain can be calculated using 6.3.

$$\sigma = \frac{E_2 d_2^3}{6d_1 R(d_2+d_1)(1-v_2)} + \frac{E_1(d_2+d_1)}{2R(1-v_1)} \tag{6.1}$$

$$R = \frac{x^2}{2y} \tag{6.2}$$

$$S = \frac{\sigma}{E_1} \tag{6.3}$$

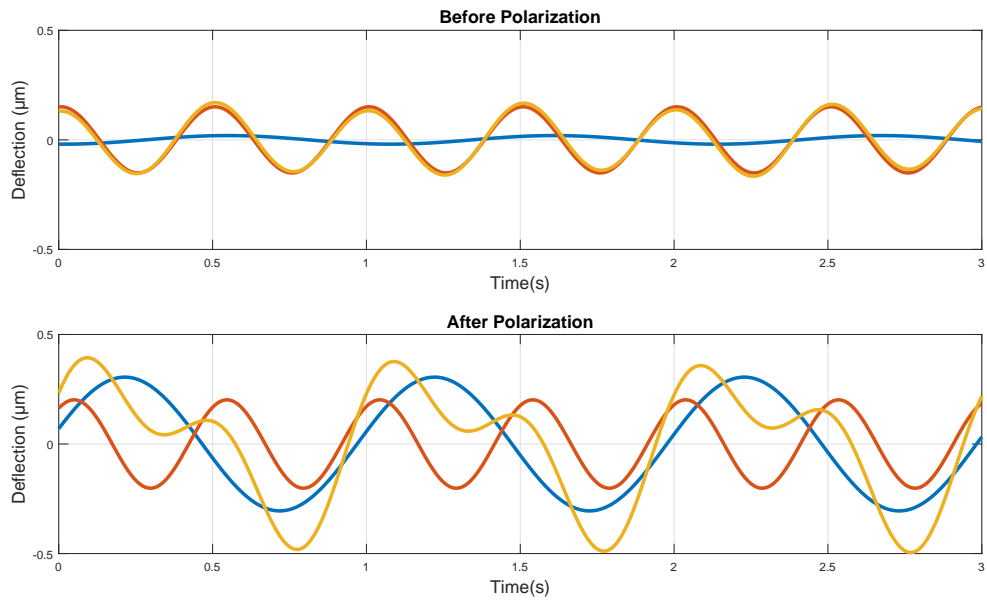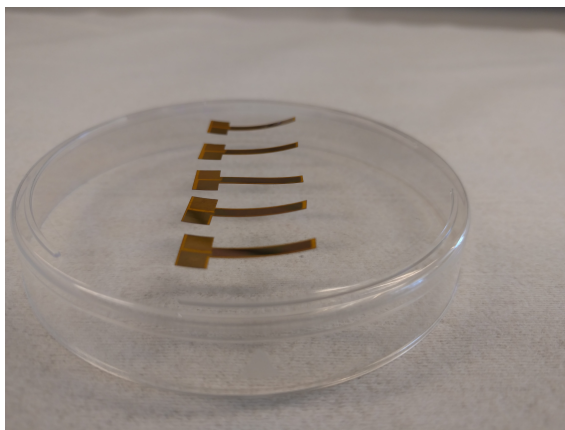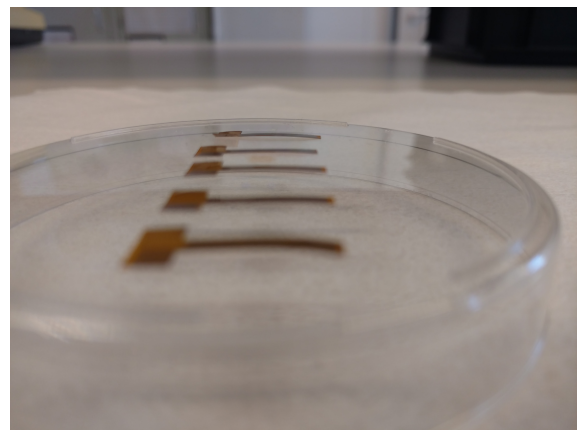Equation 6.1 can only be used with the following conditions[77]:

Figure 6.10: Deflection curve of samples 15mm long 2.6mm wide before and after solvent polarisation under 100V for 25min. Red is the electrostrictive response, blue is the piezoelectric response and yellow is the added total.

(a) Samples produced with spincasted and cured in a vacuum oven.

(b) Samples treated with a solvent annealing step before vacuum annealing.

Figure 6.11: Samples with (left) and without (right) residual stress as a result of production steps.
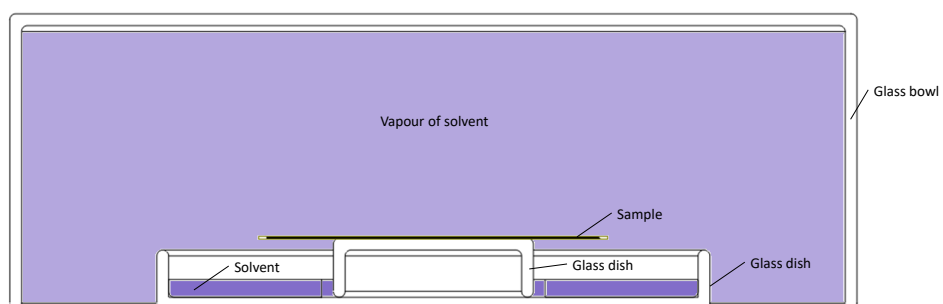

Figure 6.12: Solvent annealing setup. A large glass bowl covers 2 smaller glass containers. the medium container contains the solvent, the smallest container holds the sample. The biggest container ensures that the solvent vapour stays around the sample, keeping the sample in a near-liquid state.

Table 6.1: Calculated radius of temperature annealed samples using equation 6.2. The samples all have a length of 15mm.

Sample	Height mm	Radius m^{-1}
1	5.9	0.0191
2	3.8	0.0296
3	4.5	0.025
4	5.0	0.0225
5	5.6	0.0201
6	5.8	0.0194
7	4.9	0.023
8	5.5	0.0205
average		0.0218

1. Curvature is spherical.
2. There is no sign of de-lamination.
3. Deflection is high enough to neglect gravity.
4. Mechanical properties are isotropic in the plane of the cantilever.
5. Stress is assumed constant in the polymer layer.

The measured deflection values as a result of residual strain are reported in table 6.1, the average radius, equation 6.2, of the samples is 0.0218m. Using the data from table 6.1 an average stress can be calculated with equation 6.1, a stress value of 6.7MPa is obtained. With the stress known, using equation 6.3, an average strain of 2.2% is obtained. 2.2% residual strain or 6.7Mpa residual stress as a result of spin casting and thermal annealing is high considering the maximum strain P(VDF-TrFE-CTFE) can achieve as a result of its piezoelectric properties is 3.5%.

7

Discussion

P(VDF-TrFE-CTFE) is a special polymer indeed, the possibilities in production and tailorability are endless, the material is transparent, the electromechanical response in combination with the low Young's modulus result in interesting actuation properties. Combining all these features make this relaxor-ferroelectric polymer an interesting candidate for many different actuation applications.

The low stiffness and high dielectric properties of P(VDF-TrFE-CTFE) result in a material which serves a high electrostrictive response. Since this material allows for polarisation a piezoelectric response can be added for a total electromechanical response which is the sum of both phenomena. This piezoelectric effect increased the deflection amplitude in the lower voltage region ($30V$) from .06% to .19% strain after polarisation with $17.5V/\mu m$. Polarisation always increases the electromechanical response, it also changes the shape of the output signal. A summary of these results are listed in table 7.1 and figure 7.1.

Table 7.1: Effect on polarisation for P(VDF-TrFE-CTFE)

	low voltage	high voltage
no polarisation	low electrostrictive response & no piezoelectric response	high electrostrictive response & low piezoelectric response
with polarisation	low electrostrictive response & high piezoelectric response	high electrostrictive response & high piezoelectric response

Removing the residual stress with a solvent annealing step has influence on the final shape of the cantilever. If this intermediate step is not performed the cantilevers will have residual stress and are positioned in a pre-bend shape. There are some applications where residual stress is preferred, a pre-bend shape to avoid unwanted buckle directions, or a bend cantilever that can serve as a crawling robot leg. It is preferred to remove the residual stress in order to deliver straight cantilevers for general applications/purpose.

Solvent polarisation is a new method that can be added to the long list of polarisation methods. While this method does not require a temperature increase to soften the material, the solvent might damage other polymer parts of the application. Careful selection of production order is necessary to implement this polarisation method. In the measurement results, the cantilever was polarised with the electrodes present. It was observed that the electrodes dissolved slightly. I assume that the electrodes also serve as a barrier for the solvent vapour to fully penetrate the material. While the full effect of solvent polarisation is not studied yet, this thesis has proven that the method works and shows potential. The full potential of solvent polarization can be documented using a better method which involves the basic setup of corona charging and using a broader range of samples.

Solvent annealing is a nice method to achieve a piezoelectric response without the need of polarisation, utilising the spontaneous polarisation of relaxor-ferroelectric materials. To achieve full input following motion different methods can be used. By polarising a sample the internal structure of the material is aligned. When an input signal is set to actuate the system in the same direction as the polarisation direction the input is followed without an interference from the electrostrictive response. The same effect is visible when a solvent annealing method is performed. In figure 6.9b the piezoelectric effect formed by solvent annealing
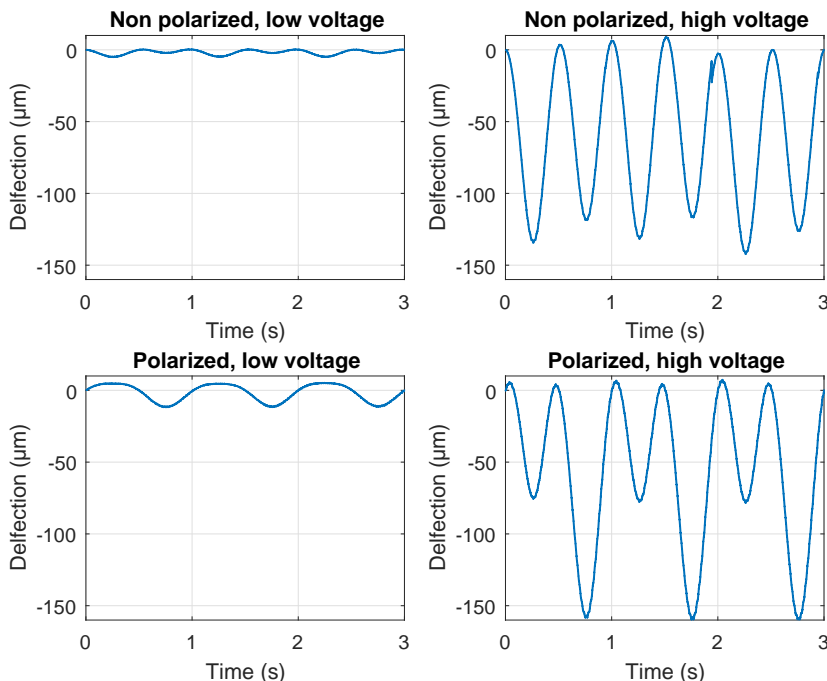
Figure 7.1: Actuator response on a 1Hz sine wave with different voltages. The left two figures are actuated with 3.75V/μm the right two figures are actuated with 8V/μm. The top two figures are not polarised, the lower two figures are polarised with 140V. The response correspond with the description in table 7.1. The result of polarisation is clearly visible in both low and high voltage applications, after polarisation the actuation amplitude is increased.

of a sample is clearly displayed. While the samples in this theses do not have a full piezoelectric response, a better setup for solvent annealing could prove if this theory is indeed true.

The reasons to choose relaxor-ferroelectric polymers over their ceramic counterparts are widely spread and maybe not even comparable. Relaxor-ferroelectric polymers have lower stiffness, are transparent and its piezoelectric coefficients are remarkable. Since they are polymers they are much more tailorable and can be processed in any desired shape. While the specifics of these polymers are improved time by time, the ultimate form has not been reached yet. Polymers w.r.t. ceramics can be spin-casted, dipped, poured or glued to mechanical systems, making them part of the material that forms a mechanical system.

The attempts in finding the recipe for multilayer P(VDF-TrFE-CTFE) actuators where not successful. The low Young's modulus might play a role in this part, P(VDF-TrFE) has a Young's modulus of 3.3Gpa while that of P(VDF-TrFE-CTFE) is 0.4Gpa. While pouring the second layer of polymer gel on top of the first layer, the first layer started to dissolve. The reason of this dissolving phenomena might be due to the low stiffness of the layer. While this method of pouring polymer gel on annealed polymer film worked neatly for P(VDF-TrFE), which has a higher Young's modulus, it did not prove successfully for P(VDF-TrFE-CTFE).

8
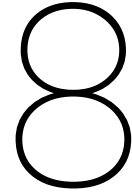
Conclusion

The Polarization effect on electromechanical response of P(VDF-TrFE-CTFE) was successfully demonstrated. By extracting the different electromechanical response from a uniform input signal the resultant output per type was defined. Using the specific response in relaxor ferroelectric material, actuators can be designed by the custom specifications of the engineer. Utilizing both uni-/bi-directional response the designer can modify the material to have an actuation path that fits its application.

The electromechanical response is not only defined by the electrostrictive coupling factor k_{31}, equation 2.2. The piezoelectric response which increases by polarization or solvent annealing also plays its part. The total electromechanical response is the summation of the electrostrictive and the piezoelectric response.

A feedforward controller to control the piezoelectric polymer was successfully designed and validated. Using the bodeplot of the theoretical model, the eigenfrequency positions and Q-factors could be determined. Combining a Notch filter with a low pass filter was sufficient to follow a triangular input signal without oscillations and significantly reduce the settling time after an step input signal.

A new method to successfully remove residual stress from thin film spin casted polymers was found. redirecting techniques readily available in the process to a new purpose has shown great influence on the residual stress in thin film polymers. Residual stress is a cause of unwanted deformation in material, removing the stress avoids the need of countermeasures and permits stress free thin film applications.

A first hint of the effect of solvent polarization was successfully performed and documented. Using the basic techniques of solvent annealing to soften a polymer material has been proven successful. Solvent polarization can be used similar to thermal polarisation where the polymer is made soft to polarize it. While thermal polarization is not always beneficial as a result of the temperature increase, solvent polarization can be used effectively as a substitute.

9

Recommendations

9.1. Future Research

9.1.1. Solvent Polarization

To increase the effect of solvent polarization, the process should be carried out with a higher electric field on the polymer. This can be done with a setup which uses corona charging as its inspiration. Combining corona charging on a sample which is made soft with a solvent vapour would increase the polarization effect in ferroelectric polymers. With corona charging no electrodes have to be sputtered on the sample making the samples cleaner for x-ray defraction. Better x-ray defraction patterns of corona polarized samples could give more clarity on the effect of solvent polarization on ferroelectric polymers.

9.1.2. Thinner films

Creating thinner films would drastically improve the deflection of cantilever structures. Using flatter substrate material and executing the whole process in a cleanroom would increase the chance of success for thin film polymers.

9.1.3. Defining blocking force

While blocking force can be calculated with the stress and stiffness of a material. Experimental verification has to be done to define the real potential of P(VDF-TrFE-CTFE). By using a force sensor or strain gauge on the tip of the cantilever the blocking force could be characterized.

9.1.4. Multilayer actuators

While in this thesis research it was not successful to make multilayer P(VDF-TrFE-CTEF), the importance of multilayer polymers to utilise the piezoelectric properties of such a material should drive the need for more research. A more structured research in to polymer structures might prove that it is indeed possible to create monolithic multilayer structures. A more thorough investigation in polymers might give the key into creating multiple layers on top of each other.

9.2. Possible applications

9.2.1. Solvent annealing to remove residual stress
Removal of internal stress might be more useful in other industries. Porous PDMS degrades over time as a result of residual stress[26], Removing the residual stress might make more stable PDMS films.

9.2.2. Crawling hexapod
The research in crawling robots is continued in every region of the world. Solutions found in complex micro mechanical structures[66][78], origami[10] and integrated actuation [79] are presented regularly. Such systems can be used in swarm technology projects, using multiple simple systems to perform one difficult task. The possibility of integrating the actuation directly in the legs of such a crawling robot could make the hexapod a monolithic design which is lightweight and cheap to produce.

9.2.3. Stiffness control for butterfly wings
Researchers at the TU Delft have developed a wing structure with a variational stick-slip system which can influence the stiffness of said wing. In this research a polymer is used and the electrostrictive forces result in a stiffening effect on the wing. The electrostrictive forces are generated with large voltages, 500 V/μm. Using P(VDF-TrFE-CTFE) those voltages can be significantly reduced by utilising the piezoelectric and electrostrictive effects of the material.

9.2.4. Transparent Acoustic transducer
Sang-Hoon Bae [19] describes the production of a transparent acoustic transducer using P(VDF-TrFE-CTFE) and graphene electrodes. The combination of graphene and P(VDF-TrFE) which are individually transparent show a transparency up to 88%. Using the inferior P(VDF-TrFE) sound was generated and measured using a microphone. Next to the purpose of transducer, the structure was tested for sensing. The sensing values from this structure show peaks up to 3V, making it a sensitive device for pressure testing. Combine the four specific features of this actuator and a transparent flexible capacitive screen which can produce sound can be created.
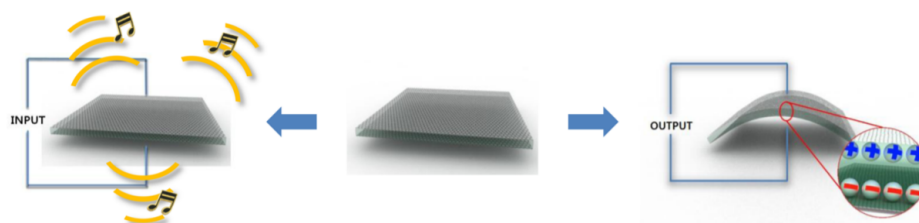

Figure 9.1: Transparant flexible transducer made with P(VDF-TrFE) and graphene. This transducer can create electrical voltage under pressure or play tunes when an electrical input is supplied. This image is directly adopted from Sang-Hoon Bae [19].

9.2.5. Liquid Varifocal Lens
Seung Tae Choi[18] describes a method to create a varifocal liquid filled microlens. This lens is created using P(VDF-TRFE-CTFE) and is thus an application which has shown its potential. The lens uses four sets of polymer actuators to change the focus in a liquid filled microlens. The achieved documented focus on targets was reported in the range of infinity to 10 cm, this was done with an operating voltage of 40V.

9.2.6. Morphing (Origami/Kirigami) Structures
Since this polymer can be casted in liquid form before it attains its solid form it is perfectly suitable for printing techniques. Screen printing has shown its effectiveness in creating large surface polymer structures[68]. Origami patterns which deform in multiple degree off freedom by actuation of on of those degrees are known in multiple occasions, similarly self folding origami structures is a research topic of high interest these days[80]. Printing P(VDF-TrFE-CTFE) on paper, cutting it into as predefined shape can enable that piece of paper into a smart origami structure which can be folded by electrical input.
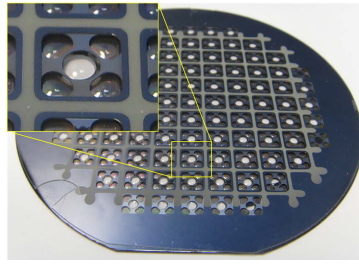
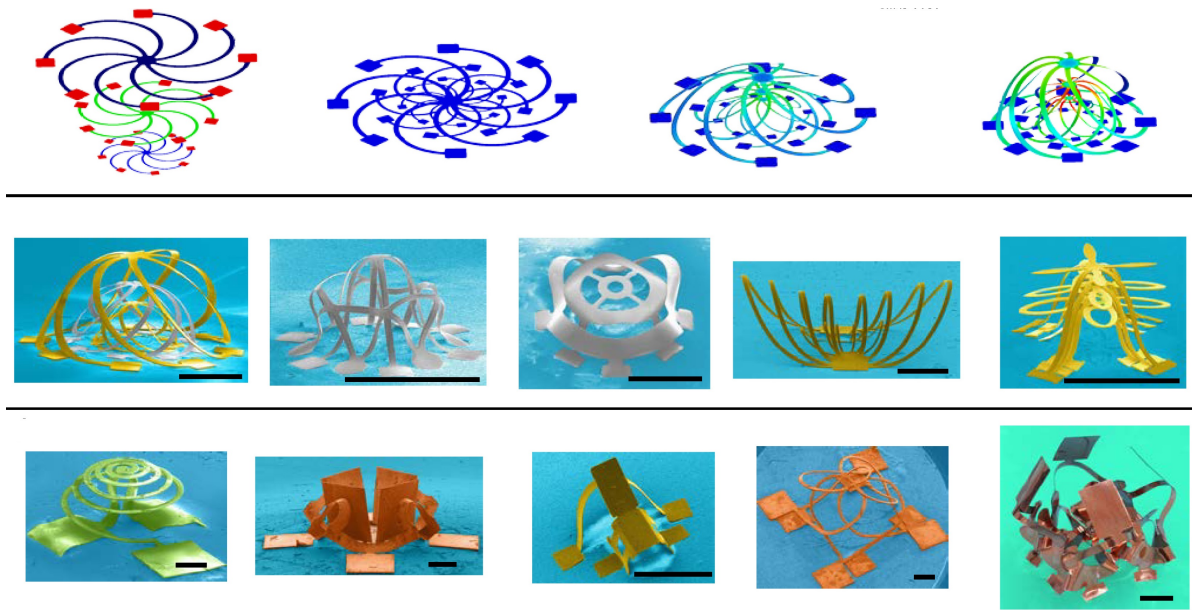Figure 9.2: Varifocal lens design by S. T. Choic[18].

Figure 9.3: Self folding structures which have the possibility to be created with P(VDF-TrFE-CTFE), this image is directly adopted from Z. Yan et al.[81].

9.2.7. Application list

Next to the previous mentioned applications a whole list of possibility's is described by Nalwa[41]. Some interesting applications are listed next.

1. Sensors
   - Accelerometers
   - Flow meters
   - Stress and strain gauges

2. Medical instrumentation
   - Artificial sensitive skin
   - Tactile sensor

3. Optical devices
   - Variable mirrors
   - Optical fiber modulators

A
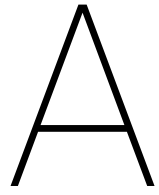
Matlab code

A.1. Generating data for model verification

The algorithms described in section 4.2 to acquire the data used to verify the models made is listed next.

```matlab
clear; close all
folder= 'storage folder';        %Set storage folder
sample='sample_#';               %Set sample name

devices = daq.getDevices;        %define DAC system
s = daq.createSession('ni');
addAnalogOutputChannel(s,'Dev1',0,'Voltage');    %define output channel
addAnalogInputChannel(s,'Dev1',0, 'Voltage');    %define input channel

Fs=50000;                                         %set Sample rate
s.Rate=Fs;                                        % −

Voltage = 50;                    %set desired output voltage
%% Generate data
amplitude=Voltage/200;           %V/amplification factor
if amplitude >= 10               %security to prevend burning of sample
disp('to high voltage, press ctl−c')
pause()
end

StopTime = 60;              % Run system for (−) seconds
t = (0:dt:StopTime−dt)';    %

output_data=idinput(length(t),'rbs',[1/(Fs/2),2000/(Fs/2)],[−amplitude amplitude]);
    %noise signal
output_data(end)=0; %always ensure zero voltage as last signal, dac will keep
    providing last signal
[P1,f] = FFT_quick(output_data,Fs);    %FFt of output data
queueOutputData(s,output_data)
subplot(3,1,1)
plot(output_data*200);
axis([0,length(output_data),−200,200])
title('Output Data Queued');
%% Run
[captured_data,time] = s.startForeground();    %Run program

%% plot
save(strcat(folder,char(strrep(strrep(strrep(datestr(now),':','_'),'−','_'),' ','_')
    ),'_Fs_',num2str(Fs),'_Sample_',sample,'_',num2str(Voltage),'V_sine','.mat'),'
    captured_data','output_data');
subplot(3,1,2)
plot(time,captured_data);
ylabel('Voltage');
xlabel('Time');
title('Acquired Signal');
[P1,f] = FFT_quick(captured_data,Fs);    %FFt of captured data
figure(1)
subplot(3,1,3)
plot(f,P1);
axis([0,100,0,0.001])
```

A.2. Model

The analytical model described in section 4 is translated to a matlab algorithm, this algorithm calculates the deflection and bodeplot.

```matlab
l=15.7e-3;                          %Length (m)
rho=[1420 8940 1780];               %Density kg/m3 [kapton copper pvdf]
width=.4e-3;                        %Width (m)
height=8;                           %Thickness(um)

d_31s=-50;                          %Dielectric constant (pm2/N)
eps_33s=14;                         %Relative permittivity (Fm^-1)
s_11=[2.7 6.3 2.7]*10^-10;          %Elastic compliance (m2/N)
h=[50 0.01 height]*10^-6;           %Thickness (m)

U=50;                               %Input Voltage (V)
r=2e-5;                             %Coefficient of friction (Ns/m)

wi=ones(1,3)*width;                 %Width (m)
thick=sum(h);                       %Total thickness (m)
mass=rho(1)*wi(1)*h(1)*l+rho(2)*wi(2)*h(2)*l+rho(3)*wi(3)*sum(h(3))*l;%Mass (kg)
mu=mass/l;                          %Mass per unit length (kg/m)
B_3=4;                              %Amplification factor(V/m)
d_31=[0 0 d_31s]*10^-12;            %Dielectric matric (m/V)

k_ml=[1.8751, 4.6941, 7.8548, 10.9955, 14.137]; %Solution to wave equation
k_m=k_ml/l;

for i =1:3                          %Center of mass (m)
a(i)=wi(i)/s_11(i)*h(i)^2;
b(i)=wi(i)/s_11(i)*h(i)*sum(h(1:i));
c(i)=wi(i)/s_11(i)*h(i);
end
z=-(sum(a)-2*sum(b))/(2*sum(c));

for i = 1:3
a(i)= wi(i)/s_11(i)*(3*h(i)*(z-sum(h(1:i)))*(z-sum(h(1:i-1)))+h(i)^3);
end

C=1/3*sum(a);                       %Flexural Rigidity (Nm^2)
n_0=l^3/C;                          %Translate of compliance (m/N)

n_m = 4*n_0./k_ml.^4;               %Torsional compliance
omega_m=(k_ml).^2./l.^2*sqrt(C/mu); % eigenfreqency
I = width*thick^3/12;               %Moment of inertia (m^4)
E = 0.3e9;                          %Youngs modulus (N/m^2 or Gpa)
omega_a = (k_ml).^2*sqrt(E*I/mu/l^4); %eigenfrequency
x=linspace(0,l,20);                 %beam (m)
kx=x'*k_m;                          %find eigenmode
                                    %Rayleigh functions
c_bar=1/2*(cosh(kx)-cos(kx));
s_bar=1/2*(sinh(kx)-sin(kx));
C_bar=1/2*(cos(k_ml)+cos(k_ml));
S_bar=1/2*(sinh(k_ml)+sin(k_ml));

for i = 3:3;
temp(i-2)= wi(i)*d_31(i)/(s_11(i)*h(i))*(2*z*h(i)-2*h(i)*sum(h(1:i))+h(i)^2);
```

```matlab
53  end
54  m_piezo=1/2*sum(temp);                  %Piezoelectric moment
55
56  X_1=(c_bar-s_bar).*C_bar./S_bar;        %Eigenmode
57
58  Y=0;
59  hu = -thick/2;
60  hl = -thick/2;
61  for i=1:3
62  hu = hu + h(i);
63  if i == 1
64  hl = hl;
65  else
66  hl = hl + h(i-1);
67  end
68  huhl(:,i)=[hu hl];
69  Y(i)=wi(i)*d_31(i)*(hu^2-hl^2)/(2*s_11(i)*h(i));%7.98
70  end
71  Y=-sum(Y);                              %Gyrator constant (C^-1)
72
73  Q=(r*l./(k_ml).^2)*sqrt(1/(C*mu));      %Q-factor (-)
74  Q=1./Q;
75  Q_list(1,:)=Q;
76
77  zeta=m_piezo*l^2/(2*C)*(x/l).^2*U;      %Deflection (m)
78
79  force= 3*C/l^3*zeta-m_piezo/(6*l)*U;    %Blocking force (N)
80
81  figure(1);subplot(3,1,1)
82  plot(x,1e6*zeta)
83  ylabel('Deflection um')
84  xlabel('length(x)');hold on
85  subplot(3,1,2)
86  plot(x,force)
87  ylabel('force N')
88  xlabel('length(x)');hold on
89  subplot(3,1,3)
90  plot(1e6*zeta,force)
91  ylabel('Force N')
92  xlabel('deflection um');hold on
93
94  f=omega_m/(2*pi);
95
96  sys_aa=(n_m(1)*X_1(:,1)'*X_1(:,1));
97  sys_ab=[1/omega_m(1)^2,1/Q(1)*1/omega_m(1),1];
98  sys_ba=(n_m(2)*X_1(:,2)'*X_1(:,2));
99  sys_bb=[1/omega_m(2)^2,1/Q(2)*1/omega_m(2),1];
100 sys_ca=(n_m(3)*X_1(:,3)'*X_1(:,3));
101 sys_cb=[1/omega_m(3)^2,1/Q(3)*1/omega_m(3),1];
102
103 sys_a = tf(sys_aa,sys_ab);
104 sys_b = tf(sys_ba,sys_bb);
105 sys_c = tf(sys_ca,sys_cb);
106
107 sys=B_3*Y*(sys_a+2.3e5*sys_b+sys_c);
108 figure(2);bode(sys,{1*2*pi,2000*2*pi}); grid on;          %deflection/input voltage
```

A.3. System verification

The acquired data in section A.1 can be processed with the tfestimate() to create a transfer function.

```matlab
close all;clear
Fs=50000; %sample rate

folder = 'storage_folder';%storage folder
d=dir(strcat(folder,char('sample_name.mat')));%sample name
[dx,dx]=sort([d.datenum]);

devi=200;%nr. of windows
for i = 1:length(d);
        lf_1=d(i).name;%sample name
        load(char(strcat(folder,string(lf_1))));%load data set
        input(:,i)=output_data*3;%amplifie voltage
        output(:,i)=captured_data*20e-6;%voltage to um
        [txy w] = tfestimate(input(:,i),detrend(output(:,i)),[length(input)/devi
            ],[],length(input),Fs);%get bode set
        sample = frd(txy,w*2*pi);%set to bode format
        save(strcat(folder,lf_1,'_divisions_',num2str(devi),'_bode.mat'),'sample');
        bode(sample,{1*2*pi,2000*2*pi});hold on %plot result
end
list = {d.name};
legend(list);
resolution = 1/(length(input)/devi/Fs);
```

A.4. Controller

The controller described in section 4.2 is composed in Matlab by making the transferfunctions listed next. Together with defining the controller, the model with the controller are simulated and plotted.

```matlab
load('C:\Users\Rens\Dropbox\Rens\Meten\Matlab\data\12\21
    _Mar_2017_13_43_21_Fs_50000_Sample_12_1.mat_divisions_250_bode.mat');%find
    dataset
bode(sample,{0.1*2*pi,1e4*2*pi});%plot measured sample
Q(1) = 10;%define Q factor, is 1/zeta
Q(2) = 1;
notch_a =[1/(2*pi*(f(1)))^2 1/(2*pi*(f(1))*Q(1)) 1];%define top half
notch_b =[1/(2*pi*f(1))^2 1/(2*pi*f(1)*Q(2)) 1];%define lower half
notch_1 = tf(notch_a, notch_b);%build notch filter

filter = tf(1,[1/(2*pi*f(1)) 1]);%low pass filter
notch = notch_1*filter*filter;%combined filter
figure()
bode(filter,notch_1,notch)%plot filters
figure(2)
bode(notch,{0.1*2*pi,1e4*2*pi});%plot filter
set(gcf, 'Position', get(0,'Screensize')); % Maximize figure.
bode(notch*sys,{0.1*2*pi,1e3*2*pi})%plot filtered model
legend('Model','Sample','Filter','Filtered model')
hold off;
figure()
step(notch_1*filter*sys);%plot filtered step response
hold on;
step(notch_1*filter*filter*sys);%plot filtered step response
step(sys);%plot unfiltered step response
```
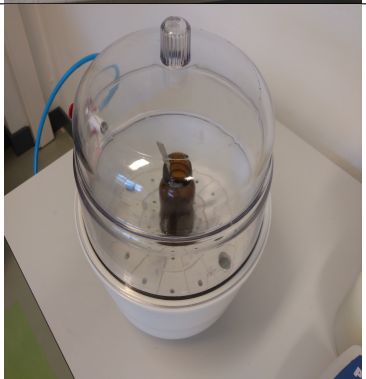
B

Production process

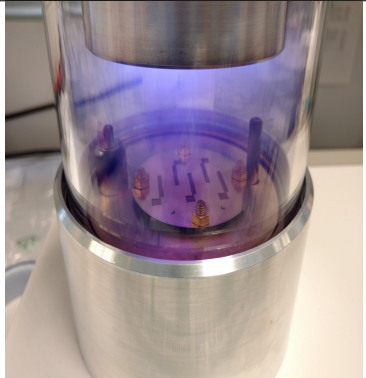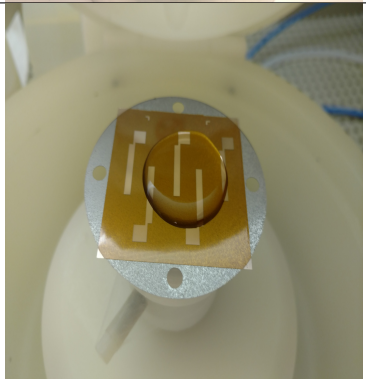| Image	Process step	Notes
	Mix polymer with solvent with a ration 10:1 (MEK to P(VDF-TrFE-CTFE)), stir for a couple of minutes to ensure a homogeneous solution.	• Apply heat (60°C) for easy mixing. • (don't use heat when using the thermal annealing process.) • Stir for minimal 5 minutes. • Don't use polymer stirring rod or cans.
	Use desiccator to remove all air bubbles in the polymer mixture	• Bubbles will cause defects in the polymer layer.
	Clean the PI samples and SS baseplate's with acetone, ethanol, acetone, ethanol. Apply a thin layer of spray adhesive and glue the PI to the SS after 30 seconds.	• Dust particles as a result of improper cleaning will cause the samples to break. • Wear protective gear (mouth mask, gloves) while handeling the spray adhesive. • Carefully place the PI samples with some tweezers, this can only be done once.

Table B.1: Sample and polymer preperation

Image	Process step	Notes
	Connect the baseplate with the PI substrate to the shadow mask with nylon screws. Align the system using the L-shaped alignment features.	• Carefully tighten the nylon screws to keep the alignment's in place. • Only use straight shadow masks, any bend masks should be thrown away.
	Use a sputter coater to make an electrode layer (20+ nm with gold).	• Keep track of the temperature, to long sputtering will destroy the sample (and the sputter coater) as a result of heat.
	Put the sample with the first electrode layer on the spin coater. Apply an amount of polymer solution on the sample covering all electrodes. Set the spin coater 30seconds at 2000 rpm.	• Center the sample in the spin caster • Close the lid • Clean the spin caster from all the residual polymer.
	Thermally anneal the sample for at least 30 min to remove the residual stress in the active polymer.	• Be careful with spillage of MEK • Ensure the sample is levelled so the PI wont slide off the SS. • Keep a small opening at the lower part of the lid, now the heavier gasses (non MEK) can escape.
	Place the samples in a vacuum oven at 111°C for 12+ hours to ensure all the solvent is evaporated.	• Number your samples so you can keep track of them.

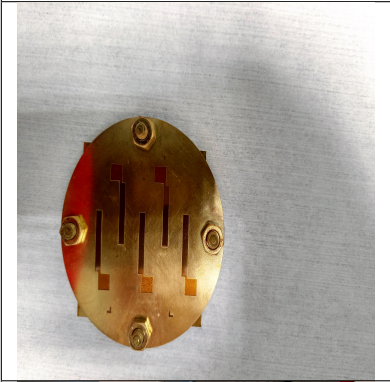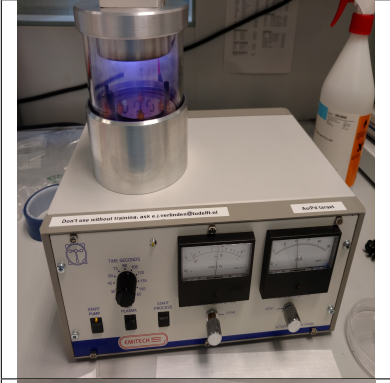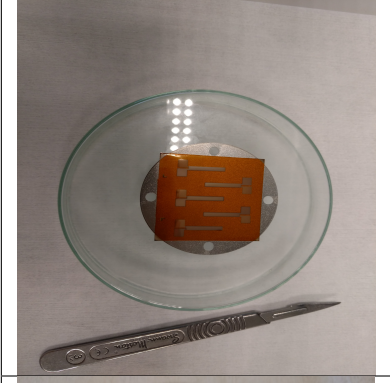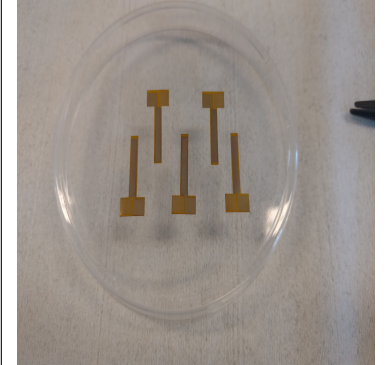Table B.2: Spin coating, sputtering and solvent annealing

Image	Process step	Notes
	Connect the baseplate with the PI substrate to the shadow mask with nylon screws. Align the system using the L-shaped alignment features.	• Carefully tighten the nylon screws to keep the alignment in place. • Only use straight shadow masks, any bend masks should be thrown away.
	Use a sputter coater to make an electrode layer (20+ nm with gold).	• Keep track of the temperature, too long sputtering will destroy the sample (and the sputter coater) as a result of heat.
	Use a scalpel to release the PI from the stainless steel baseplate.	• Use plenty of acetone to wet the blade, this will make it easier to release the PI. • Take a lot of time, any mistake will make u slice through to PI, breaking all samples.
	Use the laser cutter or a pair of scissors to precisely cut out the samples.	• Take some time make sure all settings are correct, the system is not very robust. • Handle the samples with care.

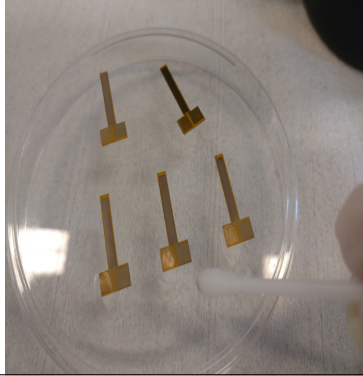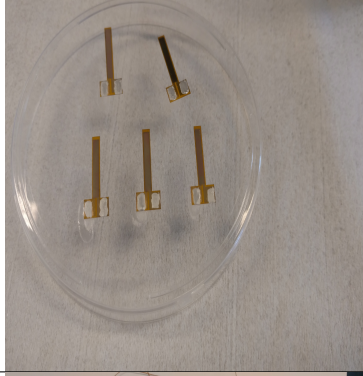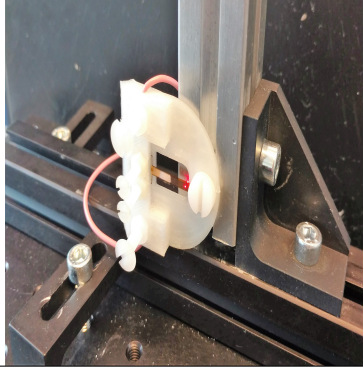Table B.3: Sputtering of electrodes and cutting of samples.

Image	Process step	Notes
	Remove the polymer layer covering the electrode with some MEK and a cue tip.	• Be very careful, MEK will dissolve the polymer. Careless handling will result in short circuit • Handle the samples with some tweezers to prevent MEK spillage from your gloves to the samples. • Use a cue tip and some MEK in a glass container.
	Apply silver paint to the electrodes to increase the contact area.	• Shake the silver bottle 30 seconds to prepare the silver paint. • Use a brush, clean it afterwards with MEK. • Apply one droplet per electrode, make them thick.
	Thermal polarization is done by connecting the electrodes to a DC source. 140V is used in this setup. Heat up the sample to 85°C and wait for 25 min. While keeping the voltage high reduce the temperature to 20°C-25°C, than remove the voltage. Replace the heating pad with the solvent setup for solvent polarization.	• Working with high voltages requires a shielded work area. • The temperature can be measured with a flexible thermocouple.
	Sample can now be used.	• Working with high voltages requires a shielded work area. • Carefully align the laser Doppler Vibrometer with the sample, the reflected laser dot has to be in the centre of the lens.

Table B.4: Silver paint and polarization

Bibliography

[1] Yoseph Bar-Cohen. Artificial muscles using electroactive polymers (eap): Capabilities, challenges and potential. 2005.

[2] Tushar Sharma, Sang-Soo Je, Brijesh Gill, and John XJ Zhang. Patterning piezoelectric thin film pvdf–trfe based pressure sensor for catheter application. *Sensors and Actuators A: physical*, 177:87–92, 2012.

[3] Kazuhiro Otsuka and Clarence Marvin Wayman. *Shape memory materials*. Cambridge university press, 1999.

[4] John DW Madden, Nathan A Vandesteeg, Patrick A Anquetil, Peter GA Madden, Arash Takshi, Rachel Z Pytel, Serge R Lafontaine, Paul A Wieringa, and Ian W Hunter. Artificial muscle technology: physical principles and naval prospects. *IEEE Journal of oceanic engineering*, 29(3):706–728, 2004.

[5] Jörg Seyfried, Marc Szymanski, Natalie Bender, Ramon Estana, Michael Thiel, and Heinz Wörn. The i-swarm project: Intelligent small world autonomous robots for micro-manipulation. In *International Workshop on Swarm Robotics*, pages 70–83. Springer, 2004.

[6] Mikołaj Rogóż, Hao Zeng, Chen Xuan, Diederik Sybolt Wiersma, and Piotr Wasylczyk. Light-driven soft robot mimics caterpillar locomotion in natural scale. *Advanced Optical Materials*, 4(11):1689–1694, 2016.

[7] Sung-Jin Park, Mattia Gazzola, Kyung Soo Park, Shirley Park, Valentina Di Santo, Erin L Blevins, Johan U Lind, Patrick H Campbell, Stephanie Dauth, Andrew K Capulli, et al. Phototactic guidance of a tissue-engineered soft-robotic ray. *Science*, 353(6295):158–162, 2016.

[8] Michael Wehner, Ryan L Truby, Daniel J Fitzgerald, Bobak Mosadegh, George M Whitesides, Jennifer A Lewis, and Robert J Wood. An integrated design and fabrication strategy for entirely soft, autonomous robots. *Nature*, 536(7617):451–455, 2016.

[9] Brigham Young University. Introduction to microelectromechanical systems (mems). Webpage, 2006. URL https://compliantmechanisms.byu.edu/content/introduction-microelectromechanical-systems-mems.

[10] Shuhei Miyashita, Steven Guitron, Marvin Ludersdorfer, Cynthia R Sung, and Daniela Rus. An untethered miniature origami robot that self-folds, walks, swims, and degrades. In *Robotics and Automation (ICRA), 2015 IEEE International Conference on*, pages 1490–1496. IEEE, 2015.

[11] Tian Qiu, Stefano Palagi, Andrew G Mark, Kai Melde, and Peer Fischer. Wireless actuator based on ultrasonic bubble streaming. In *Manipulation, Automation and Robotics at Small Scales (MARSS), International Conference on*, pages 1–5. IEEE, 2016.

[12] Sebastian Bütefisch, Volker Seidemann, and Stephanus Büttgenbach. Novel micro-pneumatic actuator for mems. *Sensors and Actuators A: Physical*, 97:638–645, 2002.

[13] F Bauer, E Fousson, QM Zhang, and LM Lee. Ferroelectric copolymers and terpolymers for electrostrictors: synthesis and properties. *IEEE transactions on dielectrics and electrical insulation*, 11(2):293–298, 2004.

[14] F Bauer, E Fousson, and QM Zhang. Recent advances in highly electrostrictive p (vdf-trfe-cfe) terpolymers. *IEEE Transactions on Dielectrics and Electrical Insulation*, 13(5):1149–1154, 2006.

[15] GS Buckley, CM Roland, R Casalini, A Petchsuk, and TC Chung. Electrostrictive properties of poly (vinylidenefluoride- trifluoroethylene- chlorotrifluoroethylene). *Chemistry of materials*, 14(6):2590–2593, 2002.

[16] Yuljae Cho, Docheon Ahn, Jong Bae Park, Sangyeon Pak, Sanghyo Lee, Byoung Ok Jun, John Hong, Su Yong Lee, Jae Eun Jang, Jinpyo Hong, et al. Enhanced ferroelectric property of p (vdf-trfe-ctfe) film using room-temperature crystallization for high-performance ferroelectric device applications. *Advanced Electronic Materials*, 2(10), 2016.

[17] O'Neil L Smith, Yunsang Kim, Mohanalingam Kathaperumal, Matthew R Gadinski, Ming-Jen Pan, Qing Wang, and Joseph W Perry. Enhanced permittivity and energy density in neat poly (vinylidene fluoride-trifluoroethylene-chlorotrifluoroethylene) terpolymer films through control of morphology. *ACS applied materials & interfaces*, 6(12):9584–9589, 2014.

[18] Seung Tae Choi, Jeong Yub Lee, Jong Oh Kwon, Seungwan Lee, and Woonbae Kim. Varifocal liquid-filled microlens operated by an electroactive polymer actuator. *Optics letters*, 36(10):1920–1922, 2011.

[19] Sang-Hoon Bae, Orhan Kahya, Bhupendra K Sharma, Junggou Kwon, Hyoung J Cho, Barbaros Ozyilmaz, and Jong-Hyun Ahn. Graphene-p (vdf-trfe) multilayer film for flexible applications. *ACS nano*, 7(4): 3130–3138, 2013.

[20] Joost van der Weijde, Bram Smit, Michael Fritschi, Cornelis van de Kamp, and Heike Vallery. Self-sensing of displacement, force and temperature for joule-heated twisted and coiled polymer muscles via electrical impedance. *IEEE/ASME Transactions on Mechatronics*, 2016.

[21] Peter Steutel. Design of a fully compliant under-actuated finger with a monolithic structure and distributed compliance. 2010.

[22] Nima Tolou, Vincent A Henneken, and Just L Herder. Statically balanced compliant micro mechanisms (sb-mems): Concepts and simulation. In *ASME 2010 International Design Engineering Technical Conferences and Computers and Information in Engineering Conference*, pages 447–454. American Society of Mechanical Engineers, 2010.

[23] Jelle Rommers, Giuseppe Radaelli, and Just Herder. A pseudo rigid body model of a single vertex compliant-facet origami mechanism (sv-cofom). In *ASME 2016 International Design Engineering Technical Conferences and Computers and Information in Engineering Conference*, pages V05BT07A006–V05BT07A006. American Society of Mechanical Engineers, 2016.

[24] Shannon A Zirbel, Robert J Lang, Mark W Thomson, Deborah A Sigel, Phillip E Walkemeyer, Brian P Trease, Spencer P Magleby, and Larry L Howell. Accommodating thickness in origami-based deployable arrays. *Journal of Mechanical Design*, 135(11):111005, 2013.

[25] Y Pauleau. Generation and evolution of residual stresses in physical vapour-deposited thin films. *Vacuum*, 61(2):175–181, 2001.

[26] Günter Reiter, Moustafa Hamieh, Pascal Damman, Séverine Sclavons, Sylvain Gabriele, Thomas Vilmin, and Elie Raphaël. Residual stresses in thin polymer films cause rupture and dominate early stages of dewetting. *Nature materials*, 4(10):754–758, 2005.

[27] Pascal Damman, Sylvain Gabriele, Séverine Coppée, Sylvain Desprez, Didier Villers, Thomas Vilmin, Elie Raphaël, Moustafa Hamieh, Samer Al Akhrass, and Günter Reiter. Relaxation of residual stress and reentanglement of polymers in spin-coated films. *Physical review letters*, 99(3):036101, 2007.

[28] SG Croll. The origin of residual internal stress in solvent-cast thermoplastic coatings. *Journal of Applied Polymer Science*, 23(3):847–858, 1979.

[29] G Reiter and PG De Gennes. Spin-cast, thin, glassy polymer films: Highly metastable forms of matter. *The European Physical Journal E: Soft Matter and Biological Physics*, 6(1):25–28, 2001.

[30] NM Kocharyan and Kh B Pachadzhyan. Study of the piezoelectric effect in poly (methyl methacrylate). In *Dokl. Akad. Nauk. Arm. SSR*, volume 36, page 277, 1963.

[31] Heiji Kawai. The piezoelectricity of poly (vinylidene fluoride). *Japanese Journal of Applied Physics*, 8(7): 975, 1969.

[32] Ken'ichi Nakamura and Yasaku Wada. Piezoelectricity, pyroelectricity, and the electrostriction constant of poly (vinylidene fluoride). *Journal of Polymer Science Part A-2: Polymer Physics*, 9(1):161–173, 1971.

[33] QM Zhang, Vivek Bharti, and X Zhao. Giant electrostriction and relaxor ferroelectric behavior in electron-irradiated poly (vinylidene fluoride-trifluoroethylene) copolymer. *Science*, 280(5372):2101–2104, 1998.

[34] Z-Y Cheng, Dana Olson, Haisheng Xu, Feng Xia, JS Hundal, QM Zhang, Fred B Bateman, GJ Kavarnos, and T Ramotowski. Structural changes and transitional behavior studied from both micro-and macroscale in the high-energy electron-irradiated poly (vinylidene fluoride-trifluoroethylene) copolymer. *Macromolecules*, 35(3):664–672, 2002.

[35] Feng Xia, Z-Y Cheng, HS Xu, HF Li, QM Zhang, George J Kavarnos, Robert Y Ting, G Abdul-Sadek, and Kevin D Belfield. High electromechanical responses in a poly (vinylidene fluoride–trifluoroethylene–chlorofluoroethylene) terpolymer. *Advanced Materials*, 14(21):1574–1577, 2002.

[36] Rüdiger G Ballas. *Piezoelectric multilayer beam bending actuators: static and dynamic behavior and aspects of sensor integration.* Springer Science & Business Media, 2007.

[37] Matthew Poulsen and Stephen Ducharme. Why ferroelectric polyvinylidene fluoride is special. *IEEE Transactions on Dielectrics and Electrical Insulation*, 17(4), 2010.

[38] Felix Gutmann. The electret. *Reviews of Modern Physics*, 20(3):457, 1948.

[39] GM Sessler. Electrical properties of polymers, 1982.

[40] P Buchman. Pyroelectric and switching properties of polyvinylidene fluoride film. *Ferroelectrics*, 5(1):39–43, 1973.

[41] Hari Singh Nalwa. *Ferroelectric polymers: chemistry: physics, and applications.* CRC Press, 1995.

[42] PKC Pillai, VK Jain, and GK Vij. Effect of polarizing temperature on the characteristics of sr10vinyl (pvc) electrets. *Journal of The Electrochemical Society*, 116(6):836–839, 1969.

[43] PKC Pillai and EL Shriver. Photoinduced polarization properties of lilo 3 single crystal. *Applied optics*, 14(12):2978–2982, 1975.

[44] Preston V Murphy, Sergio Costa Ribeiro, Fernando Milanez, and Rogerio J de Moraes. Effect of penetrating radiation on the production of persistent internal polarization in electret-forming materials. *The Journal of Chemical Physics*, 38(10):2400–2404, 1963.

[45] B Gross, GM Sessler, and JE West. Charge dynamics for electron-irradiated polymer-foil electrets. *Journal of Applied Physics*, 45(7):2841–2851, 1974.

[46] Edward A Collins, Jan Bares, and Fred W Billmeyer. Experiments in polymer science. 1973.

[47] Mototaro Eguchi. Xx. on the permanent electret. *The London, Edinburgh, and Dublin Philosophical Magazine and Journal of Science*, 49(289):178–192, 1925.

[48] John A Eldridge. Forces between magnets and between electrets. *American Journal of Physics*, 16(6):327–335, 1948.

[49] GT Davis, JE McKinney, MG Broadhurst, and SCi Roth. Electric-field-induced phase changes in poly (vinylidene fluoride). *Journal of Applied Physics*, 49(10):4998–5002, 1978.

[50] RG Kepler and RA Anderson. Ferroelectricity in polyvinylidene fluoride. *Journal of Applied Physics*, 49(3):1232–1235, 1978.

[51] Masahiko Tamura, Sumio Hagiwara, Susumu Matsumoto, and Nobuyuki Ono. Some aspects of piezoelectricity and pyroelectricity in uniaxially stretched poly (vinylidene fluoride). *Journal of Applied Physics*, 48(2):513–521, 1977.

[52] D Naegele and DY Yoon. Orientation of crystalline dipoles in poly (vinylidene fluoride) films under electric field. *Applied Physics Letters*, 33(2):132–134, 1978.

[53] Lianyun Yang, Xinyu Li, Elshad Allahyarov, Philip L Taylor, QM Zhang, and Lei Zhu. Novel polymer ferroelectric behavior via crystal isomorphism and the nanoconfinement effect. *Polymer*, 54(7):1709–1728, 2013.

[54] François Bauer. Relaxor fluorinated polymers: novel applications and recent developments. *IEEE Transactions on Dielectrics and Electrical Insulation*, 17(4), 2010.

[55] Robert W Holman and George J Kavarnos. A molecular dynamics investigation of the structural characteristics of amorphous and annealed poly (vinylidene fluoride) and vinylidene fluoride-trifluoroethylene copolymers. *Polymer*, 37(9):1697–1701, 1996.

[56] Lee J Gorny, Sheng-Guo Lu, Sheng Liu, and Minren Lin. Electromechanical properties of relaxor ferroelectric p (vdf-trfe-cfe)-p (vdf-ctfe) blends. *IEEE transactions on ultrasonics, ferroelectrics, and frequency control*, 60(3):441–445, 2013.

[57] Craig L Hom, Steven M Pilgrim, Natarajan Shankar, Keith Bridger, Mona Massuda, and Stephen R Winzer. Calculation of quasi-static electromechanical coupling coefficients for electrostrictive ceramic materials. *IEEE transactions on ultrasonics, ferroelectrics, and frequency control*, 41(4):542–551, 1994.

[58] Jean-Fabien Capsal, Jeremy Galineau, Minh-Quyen Le, Fabrice Domingues Dos Santos, and Pierre-Jean Cottinet. Enhanced electrostriction based on plasticized relaxor ferroelectric p (vdf-trfe-cfe/ctfe) blends. *Journal of Polymer Science Part B: Polymer Physics*, 53(19):1368–1379, 2015.

[59] Nellie Della Schiava, Minh-Quyen Le, Jeremy Galineau, Fabrice Domingues Dos Santos, Pierre-Jean Cottinet, and Jean-Fabien Capsal. Influence of plasticizers on the electromechanical behavior of a p (vdf-trfe-ctfe) terpolymer: Toward a high performance of electrostrictive blends. *Journal of Polymer Science Part B: Polymer Physics*, 55(4):355–369, 2017.

[60] Erik Edqvist. Polymer actuators for micro robotic applications. 2007.

[61] Jaime Martín, Dong Zhao, Thomas Lenz, Ilias Katsouras, Dago M de Leeuw, and Natalie Stingelin. Solid-state-processing of δ-pvdf. *Materials Horizons*, 2017.

[62] Cheng Huang and Qiming Zhang. High-dielectric-constant polymers as high-energy-density (hed) field effect actuator and capacitor materials. In *Smart Structures and Materials*, pages 87–98. International Society for Optics and Photonics, 2004.

[63] Stephen Timoshenko. *History of strength of materials: with a brief account of the history of theory of elasticity and theory of structures.* Courier Corporation, 1953.

[64] M Abu-Hilal. Forced vibration of euler–bernoulli beams by means of dynamic green functions. *Journal of Sound and Vibration*, 267(2):191–207, 2003.

[65] Mathworks. Mathworks - tfestimate. Webpage, 2017. URL https://nl.mathworks.com/help/signal/ref/tfestimate.html.

[66] Yeongtae Jung and Joonbum Bae. A six-legged walking robot inspired by insect locomotion. In *International Conference on Intelligent Robotics and Applications*, pages 257–264. Springer, 2013.

[67] Hugo Peters, Qi Wang, Hans Goosen, and Fred van Keulen. Active control of the hinge of a flapping wing with electrostatic sticking to modify the passive pitching motion. In *Smart Structures and Materials*, pages 153–174. Springer, 2017.

[68] Piezotech - arkema group. http://www.piezotech.eu/en/, 2017.

[69] K Norrman, A Ghanbari-Siahkali, and NB Larsen. 6 studies of spin-coated polymer films. *Annual Reports Section" C"(Physical Chemistry)*, 101:174–201, 2005.

[70] WR Blevin. Poling rates for films of polyvinylidene fluoride. *Applied Physics Letters*, 31(1):6–8, 1977.

[71] PD Southgate. Room-temperature poling and morphology changes in pyroelectric polyvinylidene fluoride. *Applied Physics Letters*, 28(5):250–252, 1976.

[72] George D. Greenwade. *The Comprehensive Tex Archive Network (CTAN)*. Polytec, https://mnelab.3me.tudelft.nl/Document/Download/111, 1 edition, 1993.

[73] Moonhor Ree, Cheng-Wu Chu, and Martin J Goldberg. Influences of chain rigidity, in-plane orientation, and thickness on residual stress of polymer films. *Journal of applied physics*, 75(3):1410–1419, 1994.

[74] MH Yang, SY Hou, YL Chang, and AC-M Yang. Molecular recoiling in polymer thin film dewetting. *Physical review letters*, 96(6):066105, 2006.

[75] GB McKenna. Size and confinement effects in glass forming liquids: Perspectives on bulk and nano-scale behaviours. *Le Journal de Physique IV*, 10(PR7):Pr7–53, 2000.

[76] EM Corcoran. Determining stresses in organic coatings using plate beam deflection. *Journal of Paint Technology*, 41(538):635–+, 1969.

[77] SG Croll and National Research Council Canada. Division of Building Research. *Internal stress in a solvent-cast thermoplastic coating*. Division of Building Research, National Research Council, 1978.

[78] Paul Birkmeyer, Kevin Peterson, and Ronald S Fearing. Dash: A dynamic 16g hexapedal robot. In *Intelligent Robots and Systems, 2009. IROS 2009. IEEE/RSJ International Conference on*, pages 2683–2689. IEEE, 2009.

[79] Niklas Snis, Erik Edqvist, Urban Simu, and Stefan Johansson. Monolithic fabrication of multilayer p (vdf-trfe) cantilevers. *Sensors and Actuators A: Physical*, 144(2):314–320, 2008.

[80] Yan Shi, Fan Zhang, Kewang Nan, Xueju Wang, Juntong Wang, Yijie Zhang, Yutong Zhang, Haiwen Luan, Keh-Chih Hwang, Yonggang Huang, et al. Plasticity-induced origami for assembly of three dimensional metallic structures guided by compressive buckling. *Extreme Mechanics Letters*, 11:105–110, 2017.

[81] Zheng Yan, Mengdi Han, Yiyuan Yang, Kewang Nan, Haiwen Luan, Yiyue Luo, Yihui Zhang, Yonggang Huang, and John A Rogers. Deterministic assembly of 3d mesostructures in advanced materials via compressive buckling: A short review of recent progress. *Extreme Mechanics Letters*, 2016.

[82] Jerry March. *Advanced organic chemistry: reactions, mechanisms, and structure*. John Wiley & Sons,, 1992.